

Lawrence Berkeley National Laboratory

Recent Work

Title

LIQUID-GAS PHASE INSTABILITIES AND DROPLET FORMATION IN NUCLEAR REACTIONS

Permalink

<https://escholarship.org/uc/item/10h6590t>

Authors

Goodman, A.L.

Kapusta, J.I.

Mekjian, A.Z.

Publication Date

1983-08-01



Lawrence Berkeley Laboratory

UNIVERSITY OF CALIFORNIA

RECEIVED
LAWRENCE
BERKELEY LABORATORY

JAN 17 1984

LIBRARY AND
DOCUMENTS SECTION

Submitted to Physical Review C

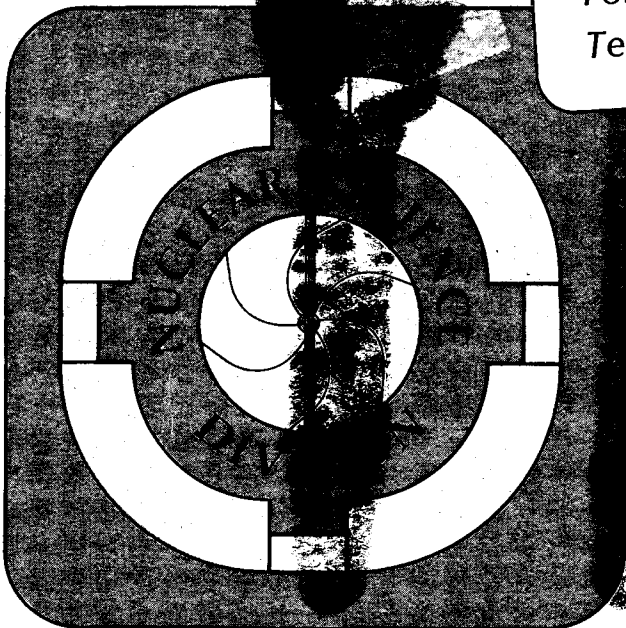
LIQUID-GAS PHASE INSTABILITIES AND DROPLET
FORMATION IN NUCLEAR REACTIONS

A.L. Goodman, J.I. Kapusta, and A.Z. Mekjian

August 1983

TWO-WEEK LOAN COPY

*This is a Library Circulating Copy
which may be borrowed for two weeks.
For a personal retention copy, call
Tech. Info. Division, Ext. 6782.*



LBL-16471
e.g.

DISCLAIMER

This document was prepared as an account of work sponsored by the United States Government. While this document is believed to contain correct information, neither the United States Government nor any agency thereof, nor the Regents of the University of California, nor any of their employees, makes any warranty, express or implied, or assumes any legal responsibility for the accuracy, completeness, or usefulness of any information, apparatus, product, or process disclosed, or represents that its use would not infringe privately owned rights. Reference herein to any specific commercial product, process, or service by its trade name, trademark, manufacturer, or otherwise, does not necessarily constitute or imply its endorsement, recommendation, or favoring by the United States Government or any agency thereof, or the Regents of the University of California. The views and opinions of authors expressed herein do not necessarily state or reflect those of the United States Government or any agency thereof or the Regents of the University of California.

LIQUID-GAS PHASE INSTABILITIES AND DROPLET
FORMATION IN NUCLEAR REACTIONS

Alan L. Goodman

Physics Department and Quantum Theory Group
Tulane University
New Orleans, Louisiana 70118*
and
Nuclear Science Division
Lawrence Berkeley Laboratory
University of California
Berkeley, California 94720

Joseph I. Kapusta

Nuclear Science Division
Lawrence Berkeley Laboratory
University of California
Berkeley, California 94720
and
School of Physics and Astronomy
University of Minnesota
Minneapolis, Minnesota 55455*

Aram Z. Mekjian

Nuclear Science Division
Lawrence Berkeley Laboratory
University of California
Berkeley, California 94720
and
Rutgers University
Department of Physics
Piscataway, N.J. 00854*

*Present addresses.

Abstract

The thermodynamics and critical exponents of nuclear matter near the critical point of a liquid-gas phase transition are studied. We then investigate fluctuations near the critical point. One effect of a finite number of nucleons, as in nuclear reactions, is to wash out the first-order phase transition for several MeV below the critical temperature. This is manifested in the fact that there is a finite probability for the system to exist in the metastable or unstable regions of infinite matter. The phenomenological droplet model is applied to a wide range of recent data on fragment yields in the range $6 < A < 52$, and good fits are obtained. Heavy ion reactions are consistent with droplet formation in a supersaturated vapor, with supersaturation ratios up to 3.25. Proton-nucleus reactions are consistent with droplet formation in a saturated vapor.

August 1983

1. Introduction

The primary goal for colliding nuclei at high energy is to study the hadronic matter equation of state. The most interesting aspect of such investigations would be to observe the consequences of a phase transition. Current theories of hadronic matter qualitatively predict the phase structure shown in Fig. 1. At high temperature or density there should be a first order phase transition to quark-gluon matter. At low temperature but high density there may be a second order phase transition to a pion-condensed state of nuclear matter. At even lower temperatures and subnuclear densities there should be a first order liquid-gas type of phase transition, terminating in a second order phase transition at the critical point. It is this last phase change to which we shall turn our attention in this paper.

There are two fundamental obstacles to realizing the aforementioned goal. First, by their very nature nuclear reactions are time-dependent phenomena and it is not immediately apparent whether or not there is sufficient time to reach a state of thermal and chemical equilibrium. Even if there is, the system must expand and pass out of the state of equilibrium. How does the system break apart? Will there be any observable consequences if a phase transition occurred? Second, nuclei are not macroscopic objects in the sense of being composed of 10^{23} particles. To what extent may one speak of thermal and chemical equilibrium for a finite number of particles? Sharp phase transitions only occur for macroscopic systems. How much would a phase transition be washed out due to finite particle number effects?

These are serious and difficult questions which may not be answered with complete satisfaction for a long time. In this paper we hope to make some theoretical and phenomenological contributions to this continuing study. We begin in Section 2 by reviewing some properties of the nuclear matter equation of state in the temperature and density domain of interest, namely $T \lesssim 20$ MeV and $\rho \lesssim \rho_0$ (normal density). Particular attention is paid to the thermodynamic behavior near the critical point including the relevant critical exponents.

In Section 3 we study for the first time the importance of finite particle number for the sharpness of the liquid-gas phase transition. For a finite number of nucleons there is a finite probability that, at a given pressure and a given temperature, the system will actually be at any density. The probability that the system is at any density other than the thermodynamically favored one decreases exponentially with the total number of particles. These density fluctuations are evaluated near the critical point with the aid of Landau's theory. The basic result is that the critical temperature can only be located to within one or two MeV given the fact that nuclear reactions are limited to 100-500 nucleons. Fluctuations in the total energy of the system are also investigated. This will give some estimate of the range in beam energy over which experimental observables will be smeared.

In Section 4 the phenomenological droplet model used in homogeneous nucleation theory of saturated and supersaturated vapors is reviewed. The droplet model is then used in a phenomenological study

of mass yields in the range $6 \leq A \leq 52$ for proton-nucleus and nucleus-nucleus collisions over a wide energy range. Fits to the data are quite satisfactory. The values of the parameters are consistent within theoretically expected ranges. The proton-nucleus data is consistent with no supersaturation, whereas the heavy ion data exhibit supersaturation ratios up to approximately 3.25.

We must emphasize that most of the recent interest in the liquid-gas phase transition and the droplet model of fragment production was stimulated by the high energy proton-nucleus experiment of the Fermi-lab-Purdue collaboration¹ and their own interpretation² of the data. Our application of the droplet model is more extensive and differs in some respects, but not in basic philosophy, we believe.

2. Equation of State

2.1 General features

The basic physics we are interested in depend only on the gross features of the nuclear equation of state.³ For definiteness the equation of state that will be primarily used in our investigation of nuclear condensation is one which is derived from a Skyrme type interaction. Specifically this interaction is

$$V = -t_0 \delta(\vec{r}_{12}) + \frac{t_1}{2} [\vec{k}^2 \delta(\vec{r}_{12}) + \delta(\vec{r}_{12}) \vec{k}^2] + t_2 \vec{k} \cdot \delta(\vec{r}_{12}) \vec{k} + \frac{t_3}{6} \delta(\vec{r}_{12}) \rho^\sigma \quad (2.1)$$

with $\vec{r}_{12} = \vec{r}_1 - \vec{r}_2$, $\vec{k} = (\vec{\nabla}_1 - \vec{\nabla}_2)/2$ and ρ is the density at $(\vec{r}_1 + \vec{r}_2)/2$.

The last term on the right hand side of eq. (2.1) is density dependent and is partially responsible for the saturating properties of nuclei.

The value of σ is usually taken as unity in the Skyrme interaction.

Using finite temperature Hartree-Fock theory with the above interaction an equation of state can be derived which is⁴

$$P = -a_0 \rho^2 + a_3 (1 + \sigma) \rho^{2+\sigma} + \left(1 - \frac{3}{2} \frac{\rho}{m^*} \frac{dm^*}{d\rho}\right) P_{Id}(m^*) \quad (2.2)$$

The $a_0 = (3/8)t_0$, $a_3 = (3/48)t_3$ and the m^* is the density dependent effective mass given by

$$\frac{m}{m^*} - 1 = \frac{1}{8} [3t_1 + 5t_2] m \rho \quad (2.3)$$

The m is the nucleon mass. In eq (2.2) the P_{Id} is the pressure of a non-interacting (ideal) gas. For a non-degenerate gas

$$P_{Id} = \rho T \quad (2.4)$$

When degeneracy corrections around the non-degenerate limit are included, the ideal pressure can be written as

$$P_{Id} = T \sum_n \tilde{B}_n \rho^n \quad (2.5)$$

with⁴

$$\begin{aligned}
 \tilde{B}_1 &= 1 \\
 \tilde{B}_2 &= \frac{1}{2^{5/2}} \frac{\lambda_T^3(m^*)}{g} \\
 \tilde{B}_3 &= \left(\frac{1}{8} - \frac{2}{9\sqrt{3}} \right) \frac{\lambda_T^6(m^*)}{g^2} \\
 \tilde{B}_4 &= \left(\frac{3\sqrt{6} + 5\sqrt{3} - 16}{32\sqrt{6}} \right) \frac{\lambda_T^9(m^*)}{g^3}
 \end{aligned} \tag{2.6}$$

It is important to note that the numerical coefficients in the B_n 's in eq (2.6) are small and rapidly decreasing with increasing n . This means that only a few terms have to be kept in eq. (2.5) even for $T \sim 5$ MeV and $\rho \sim \rho_0$, where ρ_0 is nuclear matter density. The $g = 4$ is the spin-isopin degeneracy factor and the $\lambda_T(m^*)$ is the thermal wavelength given by

$$\lambda_T(m^*) = \sqrt{\frac{2\pi}{m^*T}} \tag{2.7}$$

At the other extreme one has the degenerate limit. For $T = 0$, the ideal pressure is just the Fermi-gas pressure of a degenerate system which is

$$P_0 = \frac{2}{5} \rho \frac{P_F^2}{2m^*} \tag{2.8}$$

where the Fermi momentum is given by

$$g \left(\frac{P_F}{2\pi} \right)^3 = \frac{N}{V} = \rho \quad (2.9)$$

The N is the nucleon number. In eq (2.8) we have assumed non-relativistic particles. Corrections to the $T=0$ result can be obtained from the Sommerfeld expansion.⁵ Specifically, the first order correction to the degenerate limit gives

$$P = P_0 \left[1 + \frac{5\pi^2}{12} \left(\frac{T}{\epsilon_F} \right)^2 \right] \quad (2.10)$$

where $\epsilon_F = P_F^2/2m^*$ is the Fermi energy. The first order correction to the degenerate limit has the characteristic T^2 dependence in the pressure and also in the kinetic energy E_k/V where

$$\frac{E_k}{V} = \frac{3}{2} P_{Id} \quad (2.11)$$

The coefficients that appear in eq (2.2), the a_0 and a_3 , can be adjusted to give the correct saturation properties of nuclei, i.e., the correct binding energy at the correct equilibrium density. When $\sigma = 1$ and $m^*/m = 1$, $a_0 = 293.33 \text{ MeV fm}^3$ and $a_3 = 666.66 \text{ MeV fm}^6$ for an equilibrium density of $\rho_0 = .15 \text{ fm}^{-3}$ and for a binding energy of 8 MeV. With $\sigma = 1$ the compressibility coefficient $K = 224 \text{ MeV}$.

2.2 Critical Point Properties

In this subsection the critical point properties of our equation of state will be developed.⁶ We proceed in this discussion by considering the simplest case, the non-degenerate limit with $\sigma = 1$ and $m^*/m = 1$. For the temperatures and densities that are being considered, this is a reasonably good first approximation. The results of first order degeneracy corrections will then be given. As already noted⁴ higher order corrections will not significantly change these results.

It is also possible to start with the degenerate limit and carry out the correction due to finite temperature, as in eq. (2.10) and Ref. 3. For definiteness we will follow the former approach.

Our equation of state is then

$$P = -a_0 \rho^2 + 2a_3 \rho^3 + \rho kT \quad (2.12)$$

which is illustrated in Fig. 2.

For this equation the critical point is determined by $(\partial P / \partial \rho)_T = 0$, $(\partial^2 P / \partial \rho^2)_T = 0$ which gives

$$\begin{aligned}
 \rho_c^{(0)} &= \frac{a_0}{6a_3} \\
 T_c^{(0)} &= \frac{1}{6} \frac{a_0^2}{a_3} = a_0 \rho_c^{(0)} \\
 p_c^{(0)} &= \frac{1}{108} \frac{a_0^3}{a_3} = \frac{1}{3} \rho_c^{(0)} T_c^{(0)}
 \end{aligned} \tag{2.13}$$

The coefficient $1/3$ in the last equation multiplying $\rho_c^{(0)} T_c^{(0)}$ is near the value 0.375 for a Van der Waals equation of state. Expanding the equation of state eq (2.12) around the critical point $t = T - T_c^{(0)}$, $p = p - p_c^{(0)}$, $n = \rho - \rho_c^{(0)}$ the following result is derived

$$p = \rho_c^{(0)} t + t \eta + 2 a_3 \eta^3 \tag{2.14}$$

For $t < 0$, this cubic equation in η has three real roots for fixed p . The metastable boundaries are determined by the condition that $\partial p / \partial \eta = 0$. In fact for $t < 0$ the p, η curve has the characteristic S-shape of a Van der Waals equation as shown in Fig. 2. The points D, E shown in Fig. 2 are the limits of the metastable region. For densities between D and E the compressibility is negative and the system is unstable. The endpoints A and B can be obtained from the Maxwell construction of equal areas in a PV plot. This is equivalent to equating the pressures and chemical potentials of the two phases. Letting p_x be the Maxwell pressure then

$$\int_A^B (p - p_x) dV = 0 \quad (2.15)$$

Integrating by parts gives the condition

$$\int_A^B V dp = 0 \quad (2.16)$$

Near the critical point

$$\frac{V}{N} = \frac{1}{\eta + \rho_c} = \frac{1}{\rho_c} - \frac{\eta}{\rho_c^2} \quad (2.17)$$

so that

$$\int_A^B \frac{V}{N} dp = \int_{\eta_1}^{\eta_2} \eta \left(\frac{\partial p}{\partial \eta} \right)_t d\eta = 0 \quad (2.18)$$

The endpoints of the Maxwell construction are then given by

$$\eta_B^{(0)} = -\eta_A^{(0)} = \sqrt{\frac{-t}{2a_3}} \quad (2.19)$$

when use is made of eq (2.14). The point C of Fig. 2 is at $\eta_C = 0$.

The boundaries of the metastable region are given by $\partial p / \partial \eta = 0$.

They are

$$\eta_E^{(0)} = -\eta_D^{(0)} = \sqrt{\frac{-t}{6a_3}} \quad (2.20)$$

so that

$$\eta_E^{(0)} = \sqrt{3} \eta_B^{(0)} \quad \eta_D^{(0)} = \sqrt{3} \eta_A^{(0)} \quad (2.21)$$

Note that at $\eta = \eta_A$ and $\eta = \eta_B$, $p = p_C^{(0)} t$

The changes in Maxwell pressure with changes in temperature can be obtained from the Clausius-Clapeyron equation which for our case reads

$$\frac{d\tilde{t}}{d\tilde{p}_x} = \frac{NR}{3} \left(\frac{v_L - v_g}{s_L - s_g} \right) \quad (2.22)$$

where $v = V/V_C^{(0)}$. The subscript l,g are the liquid and gas endpoints on the Maxwell-construction line. The $\tilde{t} = T/T_C^{(0)}$ and $\tilde{p}_x = P/P_x$. The S_l and S_g are the entropies of the system at these points with

$$\frac{S_l - S_g}{N} = \ln(v_l/v_g) \quad (2.23)$$

The latent heat ΔQ is simply

$$\Delta Q = T(S_g - S_l) = NT \ln(v_g/v_l) \quad (2.24)$$

Near the critical point $\rho_g = \rho_C^{(0)} - \eta_1^{(0)}$, $\rho_l = \rho_C^{(0)} + \eta_1^{(0)}$ so that

$$\Delta Q \cong NT 2|\eta_A^{(0)}| \quad (2.25)$$

Since $\eta_A^{(0)} = -\sqrt{-t/2a_3}$ we have

$$\Delta Q \cong NT_C^{(0)} \sqrt{\frac{-t}{2a_3}} \propto \sqrt{-t} \quad (2.26)$$

Thus, the latent heat goes to zero as $\sqrt{-t}$ on the Maxwell construction line as does $S_g - S_l$.

It is instructive to rewrite eq (2.14) in the neighborhood of the critical point in various forms which explicitly show various critical exponents. Near a critical point, the general equation of state can be written as⁷

$$p - bt = \pm |\eta|^\delta f(t/\eta^{1/\beta}); \quad t \ll |\eta|^{1/\beta} \quad (2.27)$$

where the + sign is for $\eta > 0$ and the - sign is for $\eta < 0$. The result of eq (2.14) is of this form since eq (2.14) can be rewritten as

$$p - p_c^{(0)} t = 2a_3 \eta^3 \left(1 + \frac{t}{2a_3 \eta^2}\right) \quad (2.28)$$

so that

$$b = p_c^{(0)}$$

$$f(t/\eta^{1/\beta}) = 2a_3 \left(1 + \frac{t}{2a_3 \eta^2}\right) \quad (2.29)$$

The critical exponents δ , β are $\delta = 3$, $\beta = 1/2$. For the critical isotherm $t = 0$ and $p \sim \eta^3$. The critical exponent δ gives the behavior of the pressure as a function of $\rho - \rho_c$:

$$p - p_c^{(0)} = |\rho - p_c^{(0)}|^\delta \operatorname{sgn}(\rho - p_c) \quad (2.30)$$

It is not surprising that we find $\delta = 3$ since all mean field theories give $\delta = 3$. The cubic dependence in our theory follows easily from the condition $(\partial P / \partial \rho)_T = 0$ and $(\partial^2 P / \partial \rho^2)_T = 0$ used to obtain the critical point. Experiments show that δ for real gases is between 4 and 5.⁸ It is well known that mean field theories can give incorrect numerical values for the critical exponents. When $p = p_c$ then

$$1 + \frac{t}{2a_3 \eta^2} = 0 \quad (2.31)$$

and

$$\eta = \pm \sqrt{\frac{-t}{2a_3}} ; \quad p = p_c^{(0)} t \quad (2.32)$$

which is just the result of eq (2.19). The critical exponent β is defined by

$$\rho_l - \rho_g \propto (-\epsilon)^\beta \quad (2.33)$$

where

$$\epsilon = \frac{T - T_c^{(0)}}{T_c^{(0)}} = \frac{t}{T_c^{(0)}} \quad (2.34)$$

The $\rho_l - \rho_g$ are the Maxwell-construction endpoints so that $\rho_l - \rho_g$ goes to zero as $\epsilon \rightarrow 0$ as $\sqrt{-\epsilon}$ on the Maxwell line. In practice β turns out to be closer to 1/3. On the critical isobar $p = 0$ and

$$t = 1/\eta^3 \left(-\frac{2a_3}{p_c^{(0)}} \right) ; \quad p = 0 \quad (2.35)$$

Another way of writing the equation of state which makes explicit another critical exponent γ is⁷

$$p - bt = t^\gamma (C_1 \eta + C_3 \eta^3 t^{-2\beta} + \dots); \quad t \gg |\eta|^{1/\beta} \quad (2.36)$$

For the Skyrme equation of state near the critical point we have exactly (only 2 terms present on the right hand side of eq (2.36))

$$p - p_c^{(0)} t = t^\gamma (\eta + 2a_3 \eta^3 t^{-2\beta}) \quad (2.37)$$

With $\gamma = 1$, $\beta = 1/2$. The critical exponent γ gives the behavior of the isothermal compressibility K_T , $K_T^{-1} = -V(\partial P/\partial V)_T$

$$K_T = (\epsilon)^{-\gamma} \quad (2.38)$$

as a function of $\epsilon = (T - T_c^{(0)})/T_c^{(0)}$ above and near the critical point. The γ is observed to be larger than 1, $\gamma \sim 1.2$ to 1.3.

The specific heat at constant p varies as

$$C_p = \frac{1}{t + 6a_3 \eta^2} \quad (2.39)$$

which for states on the coexistence or Maxwell-construction curve diverge as $1/(-t)$. The specific heat at constant volume has associated with it the critical exponent α such that above and near the critical point

$$C_v \approx (+\epsilon)^\alpha \quad (2.40)$$

In our approach $\alpha = 0$. In summary $\alpha = 0$, $\beta = 1/2$, $\gamma = 1$, $\delta = 3$ in our mean field approach. By contrast, the Wilson Theory gives $\alpha = 0.08$, $\beta = 0.33$, $\gamma = 1.26$ and $\delta = 4.8$.⁹

2.3 First order degeneracy corrections

We now investigate the effect of degeneracy corrections on the critical point. The first order correction to the equation of state is

$$P = -a_0 \rho^2 + 2a_3 \rho^3 + \rho T + \frac{1}{2^{5/2}} \frac{\lambda_T^3(m)}{g} T \rho^2 \quad (2.41)$$

where the last term is the degeneracy correction and it corresponds to an increase in pressure due to the Pauli repulsion of Fermi-Dirac particles. The result of eq (2.41) can be recast as

$$P = -a_0^{(1)}(T) \rho^2 + 2a_3 \rho^3 + \rho T \quad (2.42)$$

where we have defined $a_0^{(1)}(T)$ to be

$$a_0^{(1)}(T) = a_0 - \frac{1}{2^{5/2}} \frac{\lambda_T^3(m) T}{g} \quad (2.43)$$

Our equation of state is like the non-degenerate equation with $a_0 \rightarrow a_0^{(1)}(T)$. For this equation of state the critical density is

$$\rho_c^{(1)} = \frac{a_0^{(1)}(T_c^{(1)})}{6a_3} \quad (2.44)$$

and the new critical temperature $T_C^{(1)}$ to first order in degeneracy is given by

$$\sqrt{T_C^{(1)}} = \frac{1}{2}\sqrt{T_C^{(0)}} + \frac{1}{2}\sqrt{T_C^{(0)}} \sqrt{1 - \left(\frac{2\pi}{m}\right)^{3/2} \frac{(3q_3)^{1/2}}{a_0^2 g}} \quad (2.45)$$

The $T_C^{(0)}$ is the zero-order (non-degenerate) result of eq. (2.13). The critical pressure is

$$P_C^{(1)} = \rho_C^{(1)} T_C^{(1)} - a_0^{(1)} \left(\rho_C^{(1)} \right)^2 + 2a_3 \left(\rho_C^{(1)} \right)^3 \quad (2.46)$$

Again we can expand our results around the new critical point $p = P - P_C^{(1)}$, $n = \rho - \rho_C^{(1)}$, $t = T - T_C^{(1)}$. First, we note that

$$a_0^{(1)}(T) \cong a_0^{(1)}(T_C^{(1)}) + C_0(T_C^{(1)}) \frac{t}{T_C^{(1)}} \quad (2.47)$$

where

$$C_0(T_C^{(1)}) \equiv \frac{1}{g} \frac{T_C^{(1)}}{2^{5/2}} \lambda_{T_C^{(1)}}^3 \quad (2.48)$$

The $\lambda_{T_C^{(1)}} = \lambda_{T_C^{(1)}}(m)$ is the thermal wavelength of eq. (2.7) evaluated at $T = T_C^{(1)}$. Then, using eq. (2.48) we obtain the following result for the equation of state near the critical point

$$\begin{aligned}
 p = & \eta t \left(1 - \frac{2}{2^{5/2}} \left(\frac{\lambda_{T_c^{(1)}}^3 \rho_c^{(1)}}{g} \right) \right) + 2a_3 \eta^3 \\
 & + \rho_c^{(2)} t \left(1 - \frac{1}{2^{5/2}} \left(\frac{\lambda_{T_c^{(1)}}^3 \rho_c^{(1)}}{g} \right) \right) - \left(\frac{1}{2^{5/2}} \frac{\lambda_{T_c^{(1)}}^3}{g} \right) \eta^2 t
 \end{aligned} \tag{2.49}$$

The last term in $\eta^2 t$ can be neglected compared to the other terms that appear in eq. (2.49) near the critical point. Thus

$$\begin{aligned}
 p = & \eta t \left(1 - \frac{1}{2^{5/2}} \left(\frac{\lambda_{T_c^{(1)}}^3 \rho_c^{(1)}}{g} \right) \right) \\
 & + \rho_c^{(2)} t \left(1 - \frac{1}{2^{5/2}} \left(\frac{\lambda_{T_c^{(1)}}^3 \rho_c^{(1)}}{g} \right) \right) + 2a_3 \eta^3
 \end{aligned} \tag{2.50}$$

Comparing eq. (2.50) with eq. (2.14) the effect of including degeneracy corrections to first-order is a change in the coefficients in front of the ηt and $\rho_c t$ terms. The new metastable boundary densities are now given by

$$-\eta_D^{(1)} + \eta_E^{(1)} = \sqrt{\frac{-t}{6a_3} \left(1 - \frac{1}{2^{5/2}} \left(\frac{\lambda_{T_c^{(1)}}^3 \rho_c^{(1)}}{g} \right) \right)} \tag{2.51}$$

and the endpoints of the Maxwell construction line are

$$\eta_A^{(2)} = \sqrt{3} \eta_D^{(2)} \quad \eta_B^{(2)} = -\eta_A^{(2)} \tag{2.52}$$

The Maxwell pressure is now

$$P_x^{(2)} = \rho_c^{(2)} t \left(1 - \frac{1}{2^{5/2}} \left(\frac{\lambda_{T_c^{(1)}}^3 \rho_c^{(1)}}{g} \right) \right) \tag{2.53}$$

Of course the critical indices are unchanged when degeneracy effects are included.

The critical density and temperature for $a_0 = 293.33 \text{ MeV fm}^3$ and $a_3 = 666.66 \text{ MeV fm}^6$ given in section 2.1 are $\rho_C^{(0)} = 0.0733 \text{ fm}^{-3}$, $T_C^{(0)} = 21.5 \text{ MeV}$; $\rho_C^{(1)} = 0.0614 \text{ fm}^{-3}$, $T_C^{(1)} = 15.1 \text{ MeV}$.

3. Fluctuations

3.1 General remarks and simplified discussion

In this section we will consider fluctuations in the liquid-gas phase coexistence. The nuclear equation of state discussed in the previous section describes the equilibrium states of the system and ignores the statistical fluctuations around the equilibrium states. For an infinite system these fluctuations are important only at the critical point, where large density fluctuations create the phenomena of critical opalescence. Fluctuations are not significant in an infinite system for states which differ from the critical point.

For a finite system statistical fluctuations can be important for states which are far from the critical point. We will address the following questions: Can these fluctuations wash out the first order liquid-gas phase transition for temperatures below T_c ? Can these fluctuations provide a mechanism for entering the metastable and unstable regions of the phase diagram?

In the liquid-gas phase transition the quantity which we will be concerned with is the probability of being in a state of the system which is not one of the equilibrium states on the Maxwell-construction line. The points A, B, C of Fig. 2 are equilibrium states. The probability of a fluctuation is proportional to the exponential of the total entropy change of a closed system. The entropy is connected to the volume in phase space $\Delta\Gamma$ by

$$S = \ln \Delta\Gamma \quad (3.1)$$

For a subsystem held at constant temperature and pressure, which are the relevant quantities to keep fixed if we are interested only in density fluctuations, the fluctuation probability reduces to an evaluation of

$$R = e^{-\Delta G/T} \quad (3.2)$$

where ΔG is the change in the Gibbs free energy G :

$$G = E - TS + PV \quad (3.3)$$

Using the first law of thermodynamics

$$dG = -SdT + VdP \quad (3.4)$$

For an isothermal process

$$(dG)_T = VdP \quad (3.5)$$

The change in G between two points 1 and 2 which have densities ρ_1 and ρ_2 but equal pressures $P_1 = P_2$ is then

$$G(\rho_2) - G(\rho_1) = \int_1^2 V (dP)_T = N \int_1^2 \frac{(dP)_T}{\rho} \quad (3.6)$$

The ρ 's here are connected to the P and T by the equation of state.

From the result of eq. (2.12)

$$\frac{G(\rho_2) - G(\rho_1)}{N} = \left[-2a_0\rho + \frac{3}{2}a_3\rho^2 + kT \ln \rho \right] \Big|_{\rho_1}^{\rho_2} \quad (3.7)$$

Thus the relative probability of being in state 2 compared to state 1 is

$$\frac{R(\rho_2)}{R(\rho_1)} = \left(\frac{\rho_1}{\rho_2} \right)^N e^{N \left[2 \frac{a_0}{T} (\rho_2 - \rho_1) - \frac{3}{2} \frac{a_3}{T} (\rho_2^2 - \rho_1^2) \right]} \quad (3.8)$$

An interesting situation to consider is point C in Fig. 2 compared to point A or B, A and B having the same Gibbs free energies. The point C is in the unstable region since $\partial P / \partial \rho < 0$. For a finite system fluctuations can populate state C. When T is close to the critical temperature, the probability of being in state C compared to A or B has a simple form

$$\frac{R(\rho_C)}{R(\rho_A)} = e^{-\frac{3}{4}N \frac{(T-T_C)^2}{TT_C}} \quad (3.9)$$

Figure 3 shows how this relative probability varies with temperature for $N = 100$. When the temperature is 95 percent of T_C , the relative probability is 0.82. The system has almost as much chance of being in the "unstable" state C as in the stable state A. However, $R(\rho_C)$ decreases rapidly as the temperature is reduced. When the temperature is 80 percent of T_C , the relative probability is only 0.024. The system has little chance to be in state C. Figure 3 may be used for other values of N by noting that the relative probability of eq. (3.9) is the N 'th power of a number which is less than one and which depends only on T/T_C .

An alternative way to present eq. (3.9) is given in Fig. 4, which shows the number of nucleons required at each temperature such that $R(\rho_C)/R(\rho_A) = 0.5$. The number N becomes infinite at the critical temperature and falls rapidly as the temperature is reduced. In a sharp first-order phase transition, the unstable state C would never be occupied. So Fig. 4 provides a rough measure of the critical number of nucleons required for a first-order phase transition.

The discussion so far has been restricted to states A, B and C of Fig. 2. These are the only densities permitted by the equation of state at the vapor pressure P_x . However, statistical density fluctuations are not restricted to these three densities. For a given temperature

and pressure the probability that the system has any arbitrary density ρ is given by eq. (3.2), so that

$$\frac{R(\rho_2)}{R(\rho_1)} = e^{-[G(\rho_2) - G(\rho_1)]/T} \quad (3.10)$$

It is therefore useful to know $G(\rho)$ for densities not permitted by the equation of state. This is provided by the Landau theory,¹⁰ in which ρ is treated as an independent variable not restricted by P and T . We now turn to this theory.

3.2. Landau Approach

The discussion of the fluctuations to be presented here is based on the Landau¹⁰ expansion of the Gibbs free energy. The essential feature of the Landau approach is the construction of the free energy in terms of a power series in the order parameter. The order parameter n in a liquid-gas phase transition is taken as the density difference $\rho - \rho_c$:

$$n = \rho - \rho_c \quad (3.11)$$

The ρ_c is the critical density discussed in the previous section. The Gibbs free energy is then a function of the pressure, temperature and order parameter. For each value of the pressure and temperature, the free energy surface $G(P, T, n)$ can be constructed. These energy

surfaces have maxima and minima, which give the values of the order parameter when the system is in thermal equilibrium.

At the critical point the order parameter η vanishes. For example, for ferromagnetic materials the order parameter is the magnetization while in ferroelectrics it is the polarization. Below the critical temperature there is a finite magnetization in the magnetic case since the magnetic moments are partially ordered or aligned. When T is near T_c the ordering of the spins by interactions is nearly balanced by the tendency toward a random state caused by the thermal motion. Fluctuations in the magnetization are then large because of this near balance. In the liquid-gas transition these large fluctuations give rise to the phenomena of critical opalescence. Light incident on a liquid-gas system at the critical point is strongly scattered by the large drops of liquid present.

In the neighborhood of the critical point, the Gibbs free energy is expanded in powers of the order parameter

$$G(P, T, \eta) = G_0(P, T) + \alpha(P, T)\eta + A(P, T)\eta^2 + C(P, T)\eta^3 + B(P, T)\eta^4 + \dots \quad (3.12)$$

The equation of state can be used to obtain the coefficients in eq. (3.12) since the equilibrium value of the order parameter is obtained by the condition that G be a minimum with respect to variations in η :

$$\frac{\partial G}{\partial \eta} = 0 \quad (3.13)$$

Specifically, the Landau order parameter that appears in eq. (3.12) is no longer connected to P,T by an equation of state but is now considered an independent variable. However, the equilibrium condition that G be an extremum gives the equation of state. Applying the condition of eq. (3.13) to eq. (3.12) gives

$$0 = \alpha(P,T) + 2A(P,T)\eta + 3C(P,T)\eta^3 + 4B(P,T)\eta^4 + \dots \quad (3.14)$$

which apart from an overall normalization constant D is the equation of state. The equation of state near the critical point is however

$$p - bt = a_1 \eta t + 2a_3 \eta^3 \quad (3.15)$$

where in the non-degenerate limit

$$b = \rho_C^{(0)}, \quad a_1 = 1 \quad (3.16)$$

from eq. (2.14). When first order degeneracy corrections are included

$$b = \rho_c^{(1)} \left(1 - \frac{1}{2^{5/2}} \left(\frac{\lambda_{T_c}^{(1)3} \rho_c^{(1)}}{g} \right) \right) \quad (3.17)$$

$$a_1 = \left(1 - \frac{1}{2^{3/2}} \left(\frac{\lambda_{T_c}^{(1)3} \rho_c^{(1)}}{g} \right) \right)$$

Comparing eq. (3.14) with eq. (3.15) the following identification can be made

$$\begin{aligned} \alpha(p, T) &= -(p - bt)D \\ A(p, T) &= a_1 t D = a_1 (T - T_c) D \\ B(p, T) &= \frac{a_3}{2} D \\ C(p, T) &= 0 \end{aligned} \quad (3.18)$$

The choice $D = N/\rho_c^2$ gives the correct G for the equilibrium states, the extremum values of G . The N is the number of nucleons. At the critical point $A(p, T) = 0$. The equation for G , in an order parameter expansion near the critical point, is then

$$G(p, T, \eta) = G_0(p, T) + \frac{N}{\rho_c^2} \left[-(p - bt)\eta + \frac{a_1}{2} t \eta^2 + \frac{a_3}{2} \eta^4 \right] \quad (3.19)$$

In the Landau expansion, when only η^2 and η^4 terms are present, the transition is described as second order in the Landau description. A first order transition in the Landau scheme would have η^2 , η^4 and η^6 terms. The linear term in eq. (3.19) is an external field term with

the external field h in a liquid-gas phase transition given by

$$h = p - bt \quad (3.20)$$

Note that G is symmetric under interchange $h \rightarrow -h$ and $\eta \rightarrow -\eta$. Thus, our liquid-gas phase transition is second order in the Landau scheme in an external field.

Identifying h as $p - bt$, then

$$\eta = \chi h \quad (3.21)$$

where χ is the "susceptibility" in this identification. The η of eq. (3.21) can then be defined as the induced order parameter $\eta = \eta_{\text{ind}}$ from an external field. In the ferromagnetic case h is the external magnetic field and η the induced magnetic moment, while in the ferroelectric case, h is the external electric field and η the induced electric dipole moment.

The "susceptibility" in eq. (3.21) is given by

$$\chi = \left(\frac{\partial \eta}{\partial h} \right)_{t, h \rightarrow 0} \quad (3.22)$$

Using eq. (3.15) we have

$$\left(\frac{\partial \eta}{\partial h} \right)_t = \frac{1}{a_1 t + 6a_3 \eta^2} \quad (3.23)$$

The condition $h > 0$ gives $2a_3n^2 + a_1t = 0$ so that

$$\chi = -\frac{1}{2a_3t}, \quad t < 0 \quad (3.24)$$

and

$$\chi = \frac{1}{a_3t}, \quad t > 0 \quad (3.25)$$

The "susceptibility" becomes infinite at $t = 0$ and it has the same properties as the specific heat at constant pressure or the compressibility at constant temperature.

The spontaneous order parameter, the order parameter in the absence of an external field ($h = 0$), corresponds to $p = bt$. The solution to the equation of state with $p = bt$ are points on the Maxwell-construction line. The spontaneous order parameter η_{sp} can be taken as

$$\eta_{sp} = \eta_B - \eta_C = 2\sqrt{\frac{-a_1t}{2a_3}} \quad (3.26)$$

and it goes to zero as the $\sqrt{-t}$ as one approaches the critical point. This square root behavior is just eq. (2.33) with the critical exponent $\beta = 1/2$. The values of G at $n = n_A$ and $n = n_B$ are minima while the other extremum point of G for $p = bt$ is $n = 0$, the C point in Fig. 2.

Let us now consider density fluctuations at the vapor pressure $p = bt$. From eq. (3.19) it follows that

$$G(p=bt, T, \eta) = G_0(p=bT, T) + \frac{N}{\rho_c^2} \left[\frac{a_1}{2} t \eta^2 + \frac{a_3}{2} \eta^4 \right] \quad (3.27)$$

This function is shown in Fig. 5. At the vapor pressure $G(n)$ is symmetric about $n = 0$. For $T < T_c$ there are two degenerate minima at n_A and n_B of Fig. 2 and a maximum at n_C of Fig. 2. This shows that the extrema in the Landau free energy occur at the densities given by the equation of state. As the temperature increases, the minima become shallower and closer together. At the critical temperature the three extrema merge and the surface is flat near $n = 0$, since

$$G(p=bT_c, T_c, \eta) = G_0(p=bT_c, T_c) + \frac{N}{\rho_c^2} \left[\frac{1}{2} a_3 \eta^4 \right] \quad (3.28)$$

The Landau free energy of Fig. 5 is used to calculate the probability distribution $R(\rho)$ of eq. (3.2). The result is shown in Fig. 6 for $N = 100$. For temperatures far below the critical temperature, $R(\rho)$ has two well-defined narrow peaks centered on the stable states at ρ_A and ρ_B . The probability for the unstable state is small. It is then proper to refer to a first-order phase transition from the gas state at ρ_A to the liquid state at ρ_B . However, as the temperature increases the two peaks begin to overlap, and the probability for the unstable state at ρ_C increases. When the temperature is 95 percent of T_C , then $R(\rho)$ is almost uniform over a wide range in ρ which extends through the stable, metastable and unstable regions. It is then improper to refer to a first-order phase transition from ρ_A to ρ_B .

The probability of having a statistical fluctuation that results in being at the Maxwell pressure p_x with the density of points D or E in Fig. 2, is simply

$$\frac{R(p_D)}{R(p_A)} = e^{-\frac{1}{3}N \frac{(T-T_C)^2}{T T_C}} \quad (3.29)$$

Comparing this result with that of eq. (3.9) we find

$$\frac{R(p_D)}{R(p_A)} = \left(\frac{R(p_C)}{R(p_A)} \right)^{4/9} \quad (3.30)$$

Thus, while the probability of being in the unstable region at point C might be small, the probability of being at the point p_x, ρ_D is not so small. For example, a 10 percent probability of being at p_x, ρ_C corresponds to a 36 percent probability of being at p_x, ρ_D while a 5 percent probability of being at ρ_C is associated with a 26 percent probability of being at ρ_D . Statistical fluctuations which are not so deep into the metastable region as ρ_D are even more likely.

The discussion so far has been restricted to the equilibrium vapor pressure, $p_x = bt$, or in zero external field $h = p - bt$. Then G has two degenerate minima at the symmetric endpoints of the Maxwell-construction line and a maxima at $\eta = 0$. When the external field is non-zero, or $p \neq bt$, minima are no longer degenerate. In fact, when the external field is such that the pressure is tangent to the curve in Fig. 2, at point D or E, the behavior of G as a function of the order parameter contains an inflection point and a minima. For a fixed t the pressure at $\eta = \eta_E$ is

$$p_E = bt + a_1 \eta_E t + 2a_3 \eta_E^3 \quad (3.31)$$

with

$$\eta_E = \sqrt{\frac{-a_1 t}{6a_3}} \quad (3.32)$$

The external field h is then

$$h_E = P_E - bt = \frac{2}{3} q_1 t \sqrt{\frac{-q_1 t}{6q_3}} \quad (3.33)$$

At $n = n_D$

$$h_D = -h_E \quad (3.34)$$

For example, in the non-degenerate approximation with $T = 0.91 T_C$, $P_X = 0.379$, $P_D = 0.409$ and $P_E = 0.349$, all in MeV fm^{-3} . Equation (3.19) is used to construct $G(\rho)$ for these three pressures, as shown in Fig. 7. Compare this with Fig. 2.

For $P = P_D$ the inflection point in $G(\rho)$ occurs at ρ_D and the minimum occurs at ρ_G . For $P = P_E$ the inflection point occurs at ρ_E and the minimum occurs at ρ_F . The corresponding curves are mirror images because of the symmetry $h \rightarrow -h$, $n \rightarrow -n$ in G , as already noted. Observe that the minima at ρ_G and ρ_F are deeper than the minima at ρ_A and ρ_B . This implies that the density fluctuations are smaller at states G and F than at A and B.

3.3. Energy Fluctuations

The fluctuations in energy for a system in contact with a heat reservoir maintained at a temperature T is simply

$$\Delta E^2 = T^2 C_V \quad , \quad (3.35)$$

where $C_V = (dE/dT)_V$ is the heat capacity at constant volume and $\Delta E = E - \bar{E}$, \bar{E} being the mean energy. This result follows from the canonical ensemble. In this ensemble states of different energies E_n are present with a probability

$$P_n = \frac{e^{-E_n/T}}{Z} \quad (3.36)$$

where Z is the partition function. For a non-degenerate ideal gas $C_V = 3N/2$, and so the fluctuation in energy per particle is

$$\frac{\sqrt{\Delta E^2}}{N} = \sqrt{\frac{3}{2N}} T \quad (3.37)$$

The ratio of the fluctuation to the mean kinetic energy is

$$\frac{\sqrt{\Delta E^2}}{E_K} = \sqrt{\frac{2}{3N}} \quad (3.38)$$

For $N = 100$ this ratio is 8.2 percent, and for $N = 500$ this ratio is 3.7 percent. This is also a good estimate for the fluctuation in temperature if the energy is held fixed,

$$\frac{\sqrt{\Delta T^2}}{T} \cong \sqrt{\frac{2}{3N}} \quad (3.39)$$

Including the first order degeneracy corrections leads to

$$\frac{\sqrt{\Delta E^2}}{E_K} = \sqrt{\frac{2}{3N}} \left(1 - \frac{5 \lambda_T^3 \rho}{2^{9/2} g} \right) \quad (3.40)$$

and so acts to reduce the fluctuations. On the other hand, starting from the degenerate limit, one arrives at

$$\frac{\sqrt{\Delta E^2}}{E_K} = \left(\frac{2}{9\pi} \right)^{1/6} \frac{g}{\lambda_T^3 \rho} \frac{1}{\sqrt{N}} \quad (3.41)$$

as $T \rightarrow 0$. Thus the relative energy fluctuation is a monotonically decreasing function of the degeneracy parameter $\lambda_T^3 \rho$. As an example, for $T = 3.5$ MeV, $\rho = \rho_0$ and $N = 100$ the ratio is 0.27 percent.

In concluding this section we may say that for a finite system statistical density fluctuations are important not only at the critical point, but in some neighborhood of the critical point. For $N = 100$ and the temperature range $0.90 \leq T/T_c \leq 1$ there are large density fluctuations which transport the system into the "unstable" region. It is then improper to speak of a first-order liquid-gas phase transition. At lower temperatures the density fluctuations diminish in amplitude, and the first-order phase transition gradually emerges.

4. Droplet Formation in a Supersaturated Vapor

4.1. General Historical Discussion

Fahrenheit initiated the study of phase equilibria and of supercooling while investigating the freezing of water.¹² Water may be supercooled and kept that way for hours. The addition of some ice, or a sudden jolt, will cause quick crystallization. Lowitz¹³ discovered the phenomenon of supersaturation in 1775, and it was subsequently shown by Gay Lussac to be a very general phenomenon.¹⁴ Again using water as an example, atmospheric cloud formation is due to condensation of water vapor on impurities or contaminants. This normally occurs when the ratio of actual vapor pressure to saturation vapor pressure (Maxwell pressure) exceeds unity by 0.01 to 0.1 of 1 percent. (This ratio is called the supersaturation ratio.) For purified air this ratio rises to about 3 whereupon condensation nuclei cause cloud formation. If these nuclei are washed out the ratio rises to 4.2. This limit is caused by negative ions. Positive ions cause the next limit at a supersaturation ratio of 6. If all of the above nucleation sites are eliminated, it is observed that fog formation occurs at a ratio of 7.9. This is attributed to homogeneous nucleation, which is the mechanism one might expect to occur in nuclear reactions.¹⁵

As a last example we mention the formation of bubbles in champagne. The nucleation sites for these bubbles are fissures in the surface of the glass bottle. (Private communication, J. Heitz, Napa Valley, California).

4.2. Droplet Model of Homogeneous Nucleation

Homogeneous nucleation occurs when chance collisions of particles in the gas phase lead to local density (or structural) inhomogeneities. These are essentially droplets of the new liquid phase. The probability of formation of these droplets can be estimated by calculating the change in the free energy of the system.¹⁵⁻¹⁸ At constant pressure and temperature the Gibbs free energy is the relevant one. Suppose that a spherical droplet contains A particles of the liquid phase and is surrounded by B particles of the gas phase. Then

$$G_{\text{with drop}} = \mu A + \mu_g B + 4\pi R^2 \sigma + T \zeta \ln A \quad (4.1)$$

and

$$G_{\text{no drop}} = \mu_g (A + B) \quad , \quad (4.2)$$

since the total number of particles $A + B$ is fixed. Here R is the radius of the drop and σ is the surface free energy. In general σ may depend on R , but usually it is assumed that R is large compared to the range of the interparticle force so that σ may be identified with the surface free energy associated with an infinite plane surface. The surface will of course have a finite thickness, with the matter on one side being in the liquid phase and on the other in the gas phase. Finally a geometric term $\ln A$ has been added to take account of the fact that the surface closes on itself which reduces the total entropy associated with the surface.¹⁷

The probability of formation of the droplet containing A particles is proportional to $\exp(-\Delta G/T)$ from eq. (3.2) with $\Delta G = G_{\text{with drop}} - G_{\text{no drop}}$, so that the yield, or density, or total number of droplets is

$$Y(A) = Y_0 \exp \left[\frac{\mu_B - \mu_A}{T} A - \frac{4\pi r^2 \sigma}{T} A^{2/3} - \mathcal{Z} \ln A \right] \quad (4.3)$$

where Y_0 is an undetermined constant. Here it has been assumed that the droplet is essentially of uniform density so that $R = rA^{1/3}$. The situation is illustrated in Fig. 8. A plot of P versus μ at fixed T shows the regions of stability, metastability and instability. At fixed μ the state with the maximum P is the thermodynamically favored one, and at fixed P is the state with the minimum μ . The density is given by the slope of the curve, namely $\rho = (\partial P / \partial \mu)_T$. One condition for thermodynamic stability is that $(\partial \rho / \partial \mu)_T > 0$, which is violated by that portion of the curve with negative curvature. When the system is sitting at the crossing point x of the pressure curve the two phases are in thermal and chemical equilibria with $\mu_g = \mu_l$. In that case

$$Y(A) = Y_0 \exp(-bA^{2/3} - \mathcal{Z} \ln A) \quad (4.4)$$

where $b = 4\pi r^2(T)\sigma(T)/T$ and $\rho^{-1} = 4\pi r^3/3$. At the critical point $b(T)$ vanishes like $^{10} (T_c - T)^{3/2}$ in the usual Van der Waals or mean field

approximation, and a little more slowly in other theories of the critical point. Specifically, the Wilson theory would give $(T_c - T)^{1.28}$.

At T_c then

$$\gamma(A) = \gamma_0 A^{-\tau} \quad (4.5)$$

which is a characteristic power-law fall-off first obtained by Fisher.¹⁷ The critical exponent τ is related to the critical exponent δ of eq. (2.27) by $\tau = 2 + \delta^{-1}$. Since, by definition of the critical point, $2 < \delta < \infty$, it must be that $2 < \tau < 2.5$. It is usually assumed that τ has no T dependence or, if it does, that τ is evaluated at T_c . In the Van der Waals model or mean field approximation $\tau = 7/3$ since $\delta = 3$, as shown in section 2.2.

The phase diagram in the temperature-density plane for a typical nuclear equation of state is shown in Fig. 9. The dashed line denotes a fixed T . Where it intersects the coexistence curve determines the densities of the gas and liquid phases. If the vapor can somehow be prepared in the supersaturated state at point g then droplets of the liquid phase will appear at point l . Points g and l correspond to the same states as in the preceding figure.

The liquid phase is much less compressible than the gas phase, as may be seen in Fig. 8. Therefore the approximation is often made of replacing μ_1 with $\mu_x(T)$ in the yield formula of eq. (4.3). In molecular physics problems it is also sometimes a good approximation to use the ideal gas relationship between chemical potential and pressure at fixed T ,

$$\mu = \text{constant} + T \ln P \quad . \quad (4.6)$$

Then $(\mu_g - \mu_x)/T = \ln(P_g/P_x)$ where P_g/P_x is the supersaturation ratio. This generally will not be a very good approximation for a nearly degenerate Fermi gas.

For any temperature less than or equal to T_c the droplet model thus predicts the generic form

$$Y = Y_0 \exp(aA - bA^{2/3} - \tau \ln A) \quad . \quad (4.7)$$

If $a = 0$, as on the coexistence curve, Y is a monotonically decreasing function of A . If $a > 0$, as in a supersaturated vapor, Y has a minimum value. The minimum is located at the critical size A_* determined by

$$a - \frac{2}{3} b A_*^{-1/3} - \frac{\tau}{A_*} = 0 \quad (4.8)$$

This corresponds to a radius

$$R_* = \frac{2\sigma}{P_g - P_x} \left\{ 1 + \frac{1}{3} (f_+(x) + f_-(x)) \right\} , \quad (4.9)$$

where

$$f_{\pm}(x) = \left[1 + x \pm 2x + x^2 \right]^{1/3} - 1, \quad (4.10)$$

$$x = \frac{27}{2} \frac{\tilde{a}_0}{\tilde{a}_2^3}, \quad (4.11)$$

$$\tilde{a}_0 = \frac{3}{4\pi} \frac{\tau}{P_g - P_x} \quad (4.12)$$

$$\tilde{a}_2 = \frac{2\sigma}{P_g - P_x} \quad (4.13)$$

The term $2\sigma/(P_g - P_x)$ in eq. (4.9) is the classic expression relating the radius, surface tension and pressure difference for spherical systems. The f 's give the corrections due to the $\tau \ln A$ term in the Gibbs free energy.

Droplets of this critical size A_* are in unstable equilibrium with the surrounding supersaturated vapor. If $A < A_*$ they tend to evaporate or breakup due to the large surface free energy, whereas if $A > A_*$ they tend to grow indefinitely. It was Gibbs¹⁹ who first realized that if a droplet of larger than critical size is formed then it threatens the existence of the gas phase since the droplet may grow indefinitely to swallow the whole system. This may then provide some insight into the kinetics of phase change, and in fact is the basis for the classical theory of homogeneous nucleation.

4.3. Law of Mass Action

At this point it is perhaps worthwhile mentioning the connection with the law-of-mass-action as it is usually applied to nuclear reactions.²⁰⁻²² Ignoring isospin, the density of ground state nuclei of mass number A is

$$\rho_{gs}(A) = g \left(\frac{mTA}{2\pi} \right)^{3/2} e^{(\mu A + B)/T} \quad (4.14)$$

where g is the spin-degeneracy and B is the total binding energy of the nucleus measured with respect to protons and neutrons. The μ is the chemical potential per nucleon associated with a particular (baryon) density of nucleons and nuclei (not the same as the density of nucleons in a nucleus). The pre-exponential factor to the $3/2$ power is associated with the free translation of the nucleus in space (kinetic energy). Not only nuclei in their ground state but also nuclei in various excited states will be present. To count them as well we multiply by the density of states $c \exp(S(E^*))$, where c is a constant and $S(E^*)$ is the entropy of the nucleus of mass number A at total excitation energy E^* , and integrate.

$$\rho(A) = \rho_{gs} \int_0^{\infty} dE^* c \exp [S(E^*) - E^*/T]. \quad (4.15)$$

The integration is usually done by saddle-point approximation. The mean excitation energy E^* is determined by the temperature.

$$\frac{dS}{dE^*} = \frac{1}{T}. \quad (4.16)$$

This leads to

$$\rho(A) = gc \left(\frac{mTA}{2\pi} \right)^{3/2} \left(\frac{\pi}{-S''(E^*)} \right)^{1/2} \exp \left\{ \mu A - \left[\bar{E}^* - B + TS(\bar{E}^*) \right] / T \right\} \quad (4.17)$$

Apart from an internal nuclear pressure divided by the density of nucleons in the nucleus, which is usually small and hence neglected,¹⁵ the quantity in brackets [...] is none other than the Gibbs free energy of nucleons within the excited nucleus. If we associate the nuclear interior with the liquid phase, and associate the surrounding free nucleons with the vapor phase, then eq. (4.17) essentially reduces to $\rho(A) \sim \exp(-\Delta G/T)$, or eq. (4.3). As before a liquid-drop expansion of ΔG for large nuclei may be employed. However, the surface properties correspond to an interface between nuclear liquid and vapor, and not between nuclear liquid and vacuum as for isolated excited nuclei. Furthermore the pre-exponential factor in eq. (4.17) must be absorbed into the definition of \mathcal{Z} , which is still related to δ via $\mathcal{Z} = 2 + \delta^{-1}$.

4.4. Droplet Model Phenomenology of Nuclear Reactions

We will now perform a phenomenological study of nuclear reactions using the droplet model. The application of the droplet model to nuclear mass distributions was initiated by the Purdue-Fermilab collaboration.^{1,2} Imagine the following scenario.²³ A proton-nucleus or

nucleus-nucleus collision may lead to an approximately thermalized system of interacting nucleons. If as the system expands it leads to temperatures $T < T_c$ at densities $\rho < \rho_0$ then it is conceivable that the nucleonic system could be pushed into the metastable phase of super-saturated vapor. There are at least two dynamical arguments why this could occur. The system could expand hydrodynamically so quickly that it passes the coexistence curve and goes into the metastable or unstable regions of nuclear matter. Or the system could exist in those regions solely by virtue of the finite particle numbers involved as discussed in section 3. There are two necessary but perhaps not sufficient conditions for this scenario to be realized. First, the system must be heated rather uniformly. Clearly this is required for the applicability of the droplet model as formulated above. Second, the system must expand quickly enough so that the competing processes of evaporation and fission do not dominate the ensemble of events. However, it must not expand too quickly otherwise thermal contact among nucleons will be lost. After some period of expansion the matter should be dilute enough and particle interactions infrequent enough that the system breaks apart. Thus the final fragment distribution should provide a rough snapshot of the state of the system at some temperature and density.

We take the above scenario as a working hypothesis. The droplet model can fit present data reasonably well, and the parameters obtained from the fit are nicely in line with theoretical expectations. Of course one would like to have a more detailed dynamic model of the time evolution of the system, but a lack of knowledge in this regard

is not without precedent. One example is that different models of the dissipation mechanism in fission lead to similar fragment energy distributions even though the time evolution of the fissioning system is quite different.²⁴ Another example is that cascade and hydrodynamic models of medium energy heavy ion collisions predict very similar inclusive single particle spectra even though the assumptions about the dynamics are quite different.²⁵

We will apply the droplet model as described in the previous section to a variety of recent data on fragment production in the range $6 \leq A \leq 52$. We will ignore the explicit effects of isospin and Coulomb energy since this is an exploratory study and since eq. (4.3) or (4.7) already has four adjustable parameters in it. Furthermore the droplets discussed above are not nuclei in their ground state but excited drops of nuclear matter which will evaporate particles to reach the ground state. This will change the isospin composition of the final fragments. A more complete calculation would involve the use of an evaporation code. This is left to future work. In view of the above, and in view of the fact that the reaction dynamics are not well understood, we will in each case determine as many of the parameters by other means as possible even though a better fit would be obtained by varying all four parameters simultaneously.

When fitting the data with eq. (4.3), the absolute normalization Y_0 is always taken as a free parameter. The critical exponent is taken to be $7/3$ as in mean field theories. As noted earlier real gases typically have slightly smaller values, about 2.2. This difference would not be noticeable with the present data. The volume coefficient

"a" measures the amount of supersaturation. Since the detailed dynamics and time evolution of the system is unknown it must be taken as a free parameter. However, for a given equation of state and for an infinite system "a" has a maximum value. This value is determined by the location of the cusp of the pressure curve at each temperature as seen in Fig. 8. The maximum value of "a" is plotted in Fig. 9 as a function of T for one particular equation of state.³ This curve gives the limit of metastability in the a-T plane which divides the regions of metastability and instability. Both the exact result $(\mu_g^{\max} - \mu_l)/T$ and the usual approximation $(\mu_g^{\max} - \mu_x)/T$ are plotted for comparison. As $T \rightarrow T_c$, $(\mu_g^{\max} - \mu_x)/T$ goes to zero like $(T_c - T)^2$. In fact near the critical point $\mu_g^{\max} = (T_c - T)^2/3T_c$, from eq. (3.29).

In the limit that the radius of the drop is large compared to the range of the internuclear force the surface coefficient $b(T)$ depends only upon the temperature. In principle it may be calculated given a particular nuclear Hamiltonian. Experimentally and theoretically it is known that at $T = 0$, $4\pi r^2 \sigma = 18$ MeV. At low temperature it decreases quadratically like $1 - \text{constant} (T/T_c)^2$, where the constant is on the order of 1-2.5.²⁶⁻²⁷ As $T \rightarrow T_c$ it vanishes like $(1 - T/T_c)^{3/2}$ in a mean field approximation, and a little more slowly in other theories, as already noted. Probably the simplest parametrization consistent with the above features is

$$b(T) = \frac{18}{T} \left(1 + \frac{3}{2} \frac{T}{T_c}\right) \left(1 - \frac{T}{T_c}\right)^{3/2}$$

(4.18)

which we shall adopt. Numerically this gives results quite similar to

the only self-consistent calculation which reaches up to $T = T_C$ we know of.²⁶ More comprehensive future studies may allow for a precise experimental determination of $\sigma(T)$.²⁸

The first data to look at is proton plus krypton reactions for beam energies of 80 to 350 GeV since the Purdue-Fermilab collaboration was the first to trigger such interest in this subject.¹ The nucleonic temperature so obtained is 14 MeV. (This is our interpretation of the data. The Purdue-Fermilab group has interpreted the slope in a different manner. See below.) (A xenon target was also used and leads to similar results.) The mass yield is shown in Fig. 11. The energy distribution for each fragment was measured and fit to a Maxwell-Boltzmann distribution modified to take into account the Coulomb energy of separation. The nucleonic temperature so obtained is 14 MeV. Using eq. (4.18) and assuming $T_C = 16$ MeV leads to the curve shown in the figure. The proton-nucleus data is consistent with $a = 0$, i.e., no supersaturation. Originally the data was fit with a pure power-law, $Y = Y_0 A^{-\tau'}$, with $\tau' = 2.65$. The latter may be called a one-shape-parameter fit whereas the former is a zero-shape-parameter fit. In fact the former provides a visibly better fit. Also our previous discussions pointed out that $2 < \tau < 2.5$ so that a fit with $\tau' = 2.65$ has a questionable interpretation. It should be pointed out that the isotopic distributions have also been measured and fit to a nuclear liquid drop type mass formula with an internal temperature of about 3.5 MeV. This need not be in disagreement with our interpretation of the data as long as one allows the hot nuclear drops to cool somewhat by gamma emission or particle evaporation.²⁹

Targets of silver and gold have been bombarded by carbon beams of energy 15 and 30 MeV per nucleon at the MSU cyclotron.³⁰ In this case only the fragment charge and not mass have been measured. The data are shown in Figs. 12 and 13. The temperature in each case has been estimated theoretically by assuming that the nuclei fuse at normal density. This provides an estimate for the surface coefficient via eq. (4.18). This leaves the volume coefficient as the only shape parameter. In line with our previous discussion on isospin we take $A = 2Z$. The best fits so obtained are also shown in the figures. Notice that the fits are quite acceptable over a range of two orders of magnitude despite the obvious simplifications inherent in the formula. For gold the critical nucleus has $A_* = 24$ for both energies. For silver $A_* = 34$ at the lower energy and $A_* = 44$ at the higher energy. These numbers may be compared to a critical droplet of water which is composed of about 40 molecules at a supersaturation ratio of 7.9. At present it is not known experimentally to what extent binary fission contributes to these yields. If it is not dominant then this data provides dramatic evidence for the supersaturation of nuclear vapor. Quantitatively similar data have been obtained in lower statistics AgBr emulsion experiments,³¹ and it has been pointed out that the minimum in the mass curve corresponds to the critical sized droplet.³²

The mass yield has been measured for neon on gold at the much higher energies of 250, 400, 1050 and 2100 MeV per nucleon. The data at 250 and 2100 MeV per nucleon are shown in Fig. 14. The data at intermediate energies have shapes midway between those two. For this whole data set the mass yield falls off more slowly than $A^{-7/3}$ so that, in

the context of the droplet model, some degree of supersaturation is indicated. Since we have no independent determination of the temperature we have assumed $T \sim T_c$ and hence $b \sim 0$. Such a low temperature is not at all inconsistent with the high beam energies, as a simple calculation shows. For example, assume that the heavy target captures the light beam nucleus, redistributes the available energy uniformly among all nucleons, and then expands hydrodynamically according to $T/T_i = (\rho/\rho_i)^{2/3}$. This leaves "a" as the only shape parameter. The best visual fits lead to the curves shown in the figure. The critical nucleus is predicted to have $A_* \sim 61$ for 250 MeV per nucleon and $A_* \sim 233$ for 2100 MeV per nucleon.

This experiment is unique in that it was capable of finding binary fission events. For the 250 MeV per nucleon collisions, it was found that for mass fragments with $80 \leq A \leq 89$ and with kinetic energies between 50 and 80 MeV, approximately 50 percent of the single particle cross section was due to binary fission. Otherwise the contribution of binary fission to the single particle inclusive cross sections was very small.

A summary of the interesting variables a, b and T is given in the table. For each reaction "a" was the only variable shape parameter. A good visual fit to the data was obtained for each reaction. This lends confidence to the interpretation of the data in terms of the droplet model. The variation of "a" with the specific reaction under consideration is noteworthy. The proton-nucleus data is consistent with little or no supersaturation, $a \sim 0$. For the heavy ion data C (or Ne) plus Au, a decreases monotonically towards zero with increasing

beam energy. In the a - T plane of Fig. 10 the fitted values of a fall within the supersaturation region, which also lends confidence to this interpretation of the data.

If we make the crude approximation that $a = \ln(P_g/P_x)$ and determine the supersaturation ratio from the data, we find values in the range 1.01 to 3.25 for the heavy ion data. The maximum value is less than one-half that observed for atmospheric fog formation.

It has been argued that if a first order phase transition occurs in heavy ion collisions the temperature and pressure balances should occur first.³⁴ The reason is that the kinetic rate constants are usually larger than the chemical rate constants (but also see Ref. 20). Thus, if $P_g = P = P$ and $T_g = T = T$, then³⁴

$$\frac{ds}{dt} = a \frac{dN_L}{dt} \quad (4.19)$$

where S is the total entropy of the system and N_L is the total number of nucleons in the liquid phase. The quantity $a = (\mu_g - \mu_l)/T > 0$ measures the amount of excess entropy generated per nucleon due to the nonequilibrium character of the phase change. The experimental indication that a is large at low beam energy may help to explain why the entropy extracted from the light fragment (p , d , t , ${}^3\text{He}$, ${}^4\text{He}$) yields is so large³ (~3.5 units of entropy).

5. Summary and Conclusions

This paper investigated properties of a possible liquid-gas phase transition in nuclei. The nuclear equation of state that we use has a characteristic Van der Waals behavior. Below a critical temperature the equation of state has a superheated and supercooled region and an unstable region. A Maxwell construction is used to describe properties of the first order liquid-gas phase transition that results from our equation of state. The critical point behavior of the system is then studied.

Fluctuations near the critical point are investigated using the Landau approach. The Gibbs free energy is expanded in terms of our order parameter which here is taken as the density difference measured from the critical point. The equilibrium states of the system correspond to the extremum of this Gibbs free energy as a function of the order parameter. Properties of the Gibbs free energy are then discussed. For example, it is shown that the liquid-gas phase transition is a second order phase transition in an external field in the Landau description for our equation of state. When the pressure of the system is the vapor pressure the Gibbs free energy has two degenerate minima and the order parameter is spontaneously broken. When pressure is not equal to the vapor pressure, an external field is present which changes the behavior of the free energy. For a particular choice of the pressure, the Gibbs free energy has an inflection point and a minimum.

Our Gibbs free energy expansion in terms of the order parameter is then used to answer the following questions: 1) For a finite system do fluctuations wash out the first order phase transition? 2) Can fluctuations take such a system into the metastable regions? For temperatures within a few MeV of the critical temperature, fluctuations into the unstable region are large. However at lower temperatures fluctuations into the metastable region are important, but states in the unstable region are not likely to be found. The sharpness of a first order liquid-gas phase transition increases as the temperature difference below the critical temperature increases in absolute magnitude.

We next turn our attention to the yields of composite nuclei seen in high energy proton-nucleus collisions and in nucleus-nucleus collisions. A phenomenological droplet model is found to describe the data on fragment yields of nuclei up to $A \approx 50$. Our picture is that such fragments correspond to droplet formation in a supersaturated vapor for nucleus-nucleus collisions and in a saturated vapor in proton-nucleus collisions. In the supersaturated case a critical size droplet exists which is determined by the surface tension and supersaturation ratio. Droplets larger than the critical drop grow by accumulating nucleons from the vapor. Droplets smaller than the critical size evaporate nucleons to the vapor. This behavior reflects itself in the yield distributions as an initial decrease to the critical size and then an increase beyond the critical size.

While we have considered statistical laws in developing expressions for droplet sizes, we have not considered the dynamical process that led to droplet formation. When the droplets are present in small numbers, the reactions between clusters and single vapor nucleons provide the mechanism for growth and evaporation of clusters. The rates for formation from the supersaturated phase to the droplet phase will be governed by "potential barriers" in the Gibbs free energy particle. Near the critical point these barriers will be small, but away from the critical point they can be quite large. We will leave the question of the kinetics of the process of droplet formation to a future paper.

Acknowledgements

This work was supported by the Director, Office of Energy Research, Division of Nuclear Physics of the Office of High Energy and Nuclear Physics of the U. S. Department of Energy under Contract No. DE-AC03-76SF00098.

References

1. J.E. Finn, S. Agarwal, A. Bujak, J. Chuang, L.J. Gutay, A.S. Hirsch, R.W. Minich, N.T. Porile, R.P. Scharenberg, B.C. Stringfellow and F. Turkot, Phys. Rev. Lett. 49, 1321 (1982).
2. R.W. Minich, S. Agarwal, A. Bujak, J. Chuang, J.E. Finn, L.J. Gutay, A.S. Hirsch, N.T. Porile, R.P. Scharenberg, B.C. Stringfellow and F. Turkot, Phys. Lett. 118B, 458 (1982).
3. J. Kapusta, University of Minnesota preprint, 1983.
4. H. Jaqaman, A.Z. Mekjian and L. Zamick, Phys. Rev. C27, 2728 (1983).
5. A. Sommerfeld, Thermodynamics and Statistical Mechanics (New York, Academic Press, 1956).
6. M.W. Curtin, H. Toki and D.K. Scott, Phys. Lett. 123B, 289 (1983).
7. B. Widom, J. Chem. Phys. 43, 3892 (1965); *ibid* p. 3898.
8. C.S. Kiang, Phys. Rev. Lett. 24, 47 (1970).
9. K.G. Wilson, Phys. Rev. B4, 3174 (1971); *ibid* p. 3184. See also Ref. 10.
10. E.M. Lifshitz and L.P. Pitaevskii, Statistical Physics (3rd English ed., Part 1, Pergamon, New York, 1980).
11. F. Reif, Fundamentals of Statistical and Thermal Physics (McGraw-Hill, 1965).
12. D.B. Fahrenheit, Phil. Trans. Roy. Soc. 39, 78 (1724).
13. J.T. Lowitz, Crelle's Chemische Annalen 1, 3 (1795).
14. J.L. Gay Lussac, Ann. de Chimie 87, 225 (1813).

15. Nucleation, edited by A.C. Zettlemoyer (Marcel Dekker, New York, 1969). This book contains a wealth of information.
16. J. Frenkel, Kinetic Theory of Liquids (Dover, 1955, New York).
17. M.E. Fisher, Physics 3, 255 (1967); in Proceedings of the International School of Physics 'Enrico Fermi,' Course LI, Critical Phenomena (edited by M.S. Green, Academic Press, 1971, New York).
18. J.E. McDonald, Amer. J. Phys. 30, 870 (1962); ibid, 31, 31 (1963).
19. J.W. Gibbs, Scientific Papers (Longmans Green, London, 1906) Vol. 1.
20. A.Z. Mekjian, Phys. Rev. C17, 1051 (1978).
21. J. Randrup and S.E. Koonin, Nucl. Phys. A356, 223 (1981).
22. G. Fáti and J. Randrup, Nucl. Phys. A381, 557 (1982).
23. G. Bertsch and P.J. Siemens, Phys. Lett. 126B, 9 (1983).
24. A.J. Sierk and J.R. Nix, Phys. Rev. C21, 982 (1980).
25. A.A. Amsden, J.N. Ginocchio, F.H. Harlow, J.R. Nix, M. Danos, E.C. Halbert and R.K. Smith, Jr., Phys. Rev. Lett. 38, 1055 (1977).
26. W.A. Küpper, Institut für Kernphysik, TH Darmstadt, Report 75/3, unpublished.
27. G. Sauer, H. Chandra and U. Mosel, Nucl. Phys. A264, 221 (1976).
28. P.J. Siemens, Texas A&M University preprint, 1983.
29. W.A. Friedman and W.G. Lynch, Phys. Rev. C28, 16 (1983).
30. C.B. Chitwood, D.J. Fields, C.K. Gelbke, W.G. Lynch, A.D. Panagiotou, M.B. Tsang, H. Utsunomiya and W.A. Friedman, Michigan State University preprint, 1983.

31. B. Jakobsson, G. Jönson, B. Lindquist and A. Oskarsson, Z. Physik A307, 293 (1982).
32. H. Stöcker, G. Buchwald, G. Graebner, P. Subramanian, J.A. Maruhn, W. Greiner, B.V. Jacak and G.D. Westfall, Nucl. Phys. A400, 63c (1983).
33. A.I. Warwick, H.H. Wieman, H.H. Gutbrod, M.R. Maier, J. Peter, H.G. Ritter, H. Stelzer, F. Weik, M. Freedman, D.J. Henderson, S.B. Kaufman, E.P. Steinberg and B.D. Wilkins, Phys. Rev. C27, 1083 (1983). We are grateful for private communication of some unpublished data.
34. L.P. Csernai and B. Lukács, University of Frankfurt preprint, 1983.

Table

Physical parameters associated with the phenomenological fits to the data in Figures 11-14.

<u>Reaction</u>		<u>T</u>	<u>b</u>	<u>a</u>	Number of variable shape parameters
C + Au	15 MeV/nucleon	3.5 MeV	4.7	1.18	1
C + Au	30 MeV/nucleon	5.0 MeV	3.0	0.79	1
Ne + Au	250 MeV/nucleon	$\sim T_c$	~ 0	0.038	1
Ne + Au	2100 MeV/nucleon	$\sim T_c$	~ 0	0.01	1
C + Ag	15 MeV/nucleon	4.6 MeV	3.3	0.77	1
C + Ag	30 MeV/nucleon	6.5 MeV	2.0	0.43	1
p + Kr	80-350 Gev	14 MeV	0.13	~ 0	0

Figure Captions

- Fig. 1 Theoretically expected phase diagram for the strong interactions. If the quark-gluon phase transition is first order then there would also be a coexistence region (not shown).
- Fig. 2 Equation of state for the liquid-gas phase transition illustrating the Maxwell-construction (dashed line). Two isotherms of pressure versus density are plotted.
- Fig. 3. R is the relative probability that the system is in the unstable state C compared to the thermodynamically favored state A (or B). The nucleon number is 100.
- Fig. 4. N is the number of nucleons required to reduce $R(\rho_C)/R(\rho_A)$ to 0.5.
- Fig. 5. The Gibbs free energy per nucleon versus the density. Each curve has a constant temperature and a constant pressure given by the equilibrium vapor pressure.
- Fig. 6. R is the relative probability for the system to be at density ρ compared to the thermodynamically favored values ρ_A and ρ_B . The pressure is the equilibrium vapor pressure. The number of nucleons is 100.

Fig. 7. The Gibbs free energy difference per nucleon versus the density. The pressure P is in units of MeV fm^{-3} .

Fig. 8. Parametric pressure - chemical potential curve at fixed temperature. The parameter is the density ρ , which is also $(\partial P / \partial \mu)_T$.

Fig. 9. Regions of stability, metastability and instability for uniform nuclear matter.

Fig. 10. Regions of metastability and instability, in terms of the volume coefficient a of eqs. (4.3) and (4.7), for a particular equation of state.³

Fig. 11. Droplet model fit to the data of Ref. 1.

Fig. 12. Droplet model fit to the data of Ref. 30.

Fig. 13. Droplet model fit to the data of Ref. 30.

Fig. 14. Droplet model fit to the data of Ref. 33.

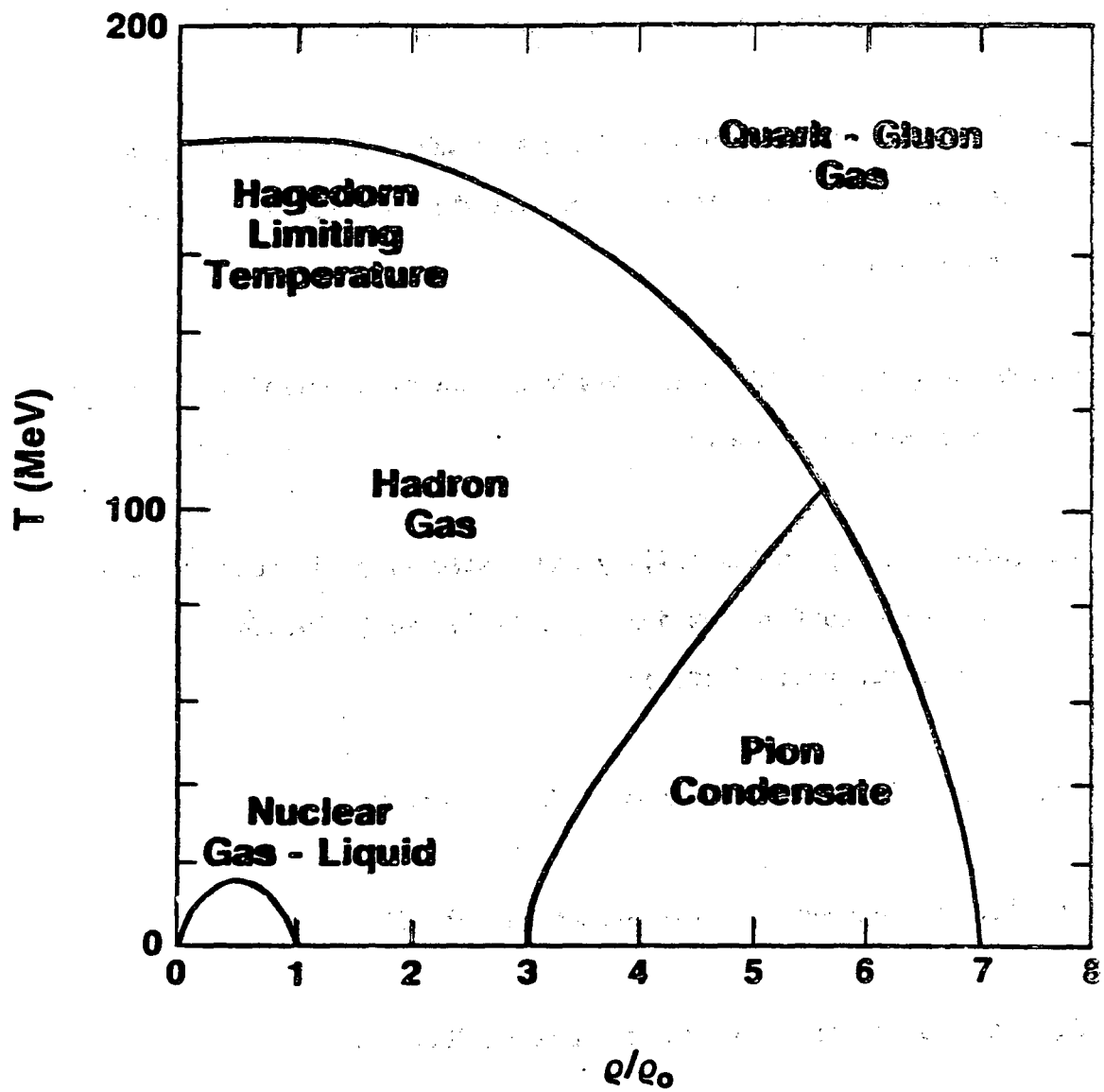


Fig. 1

XBL 838-2915

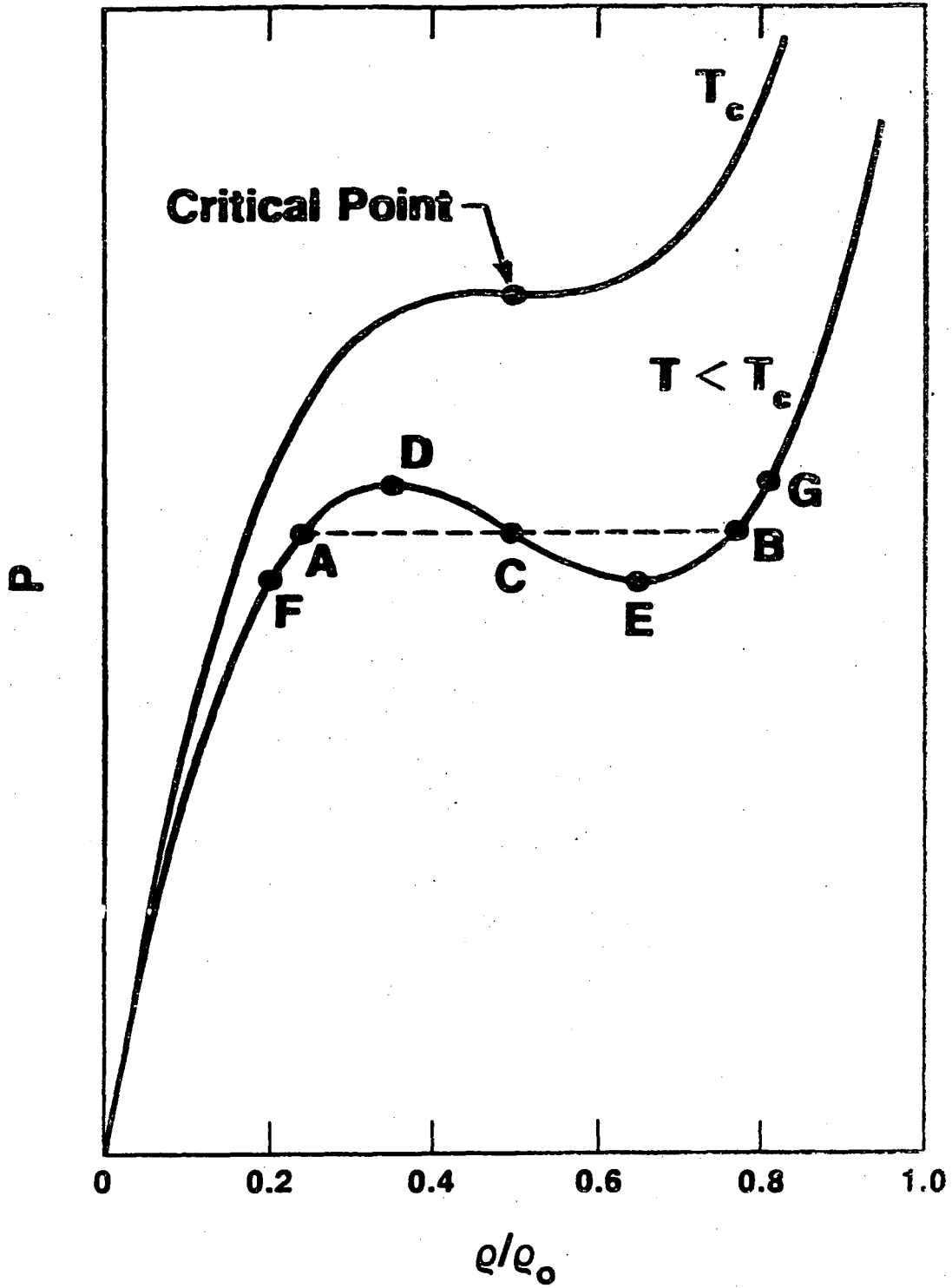


Fig. 2

XBL 838-2908

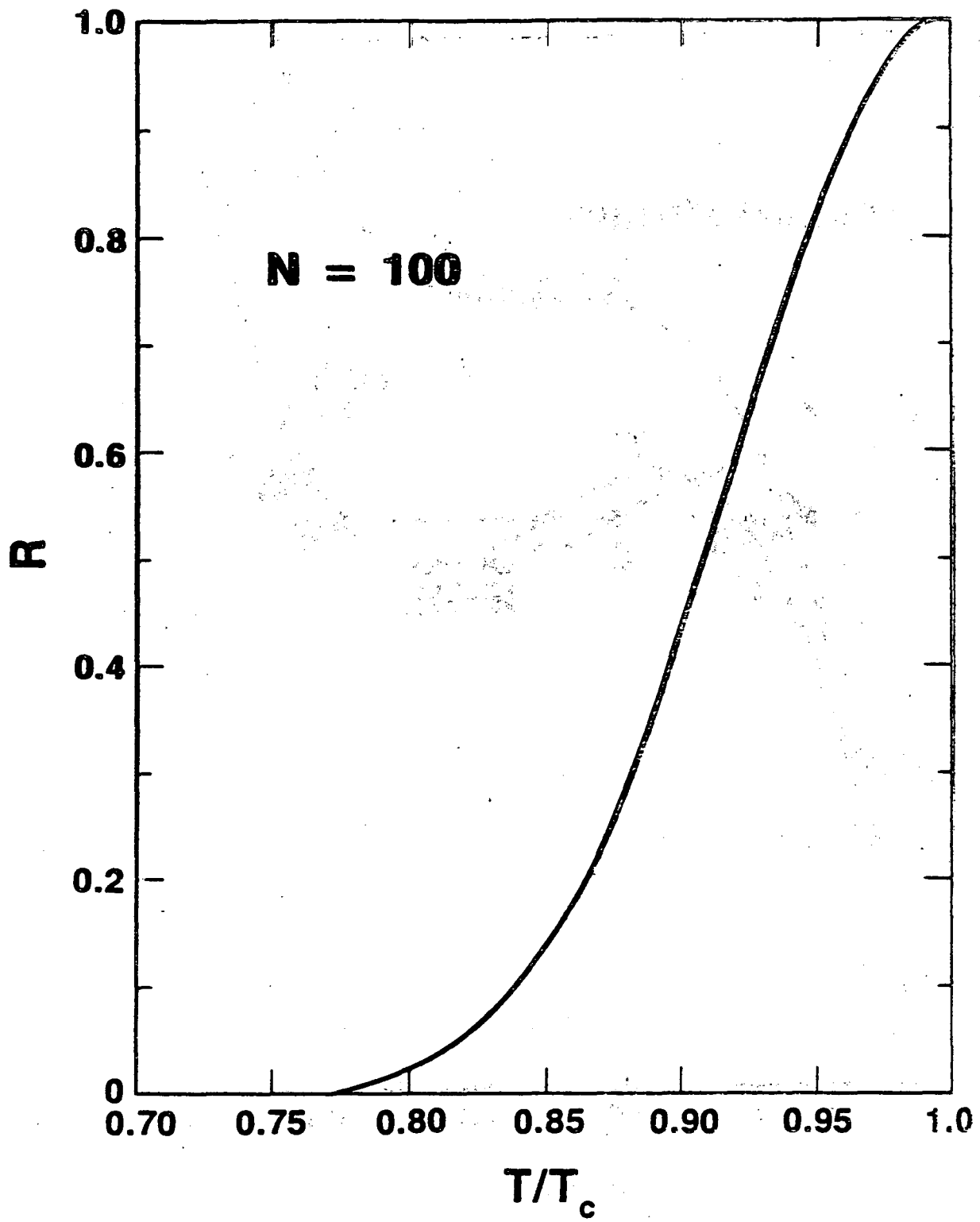


Fig. 3

XBL 838-11001

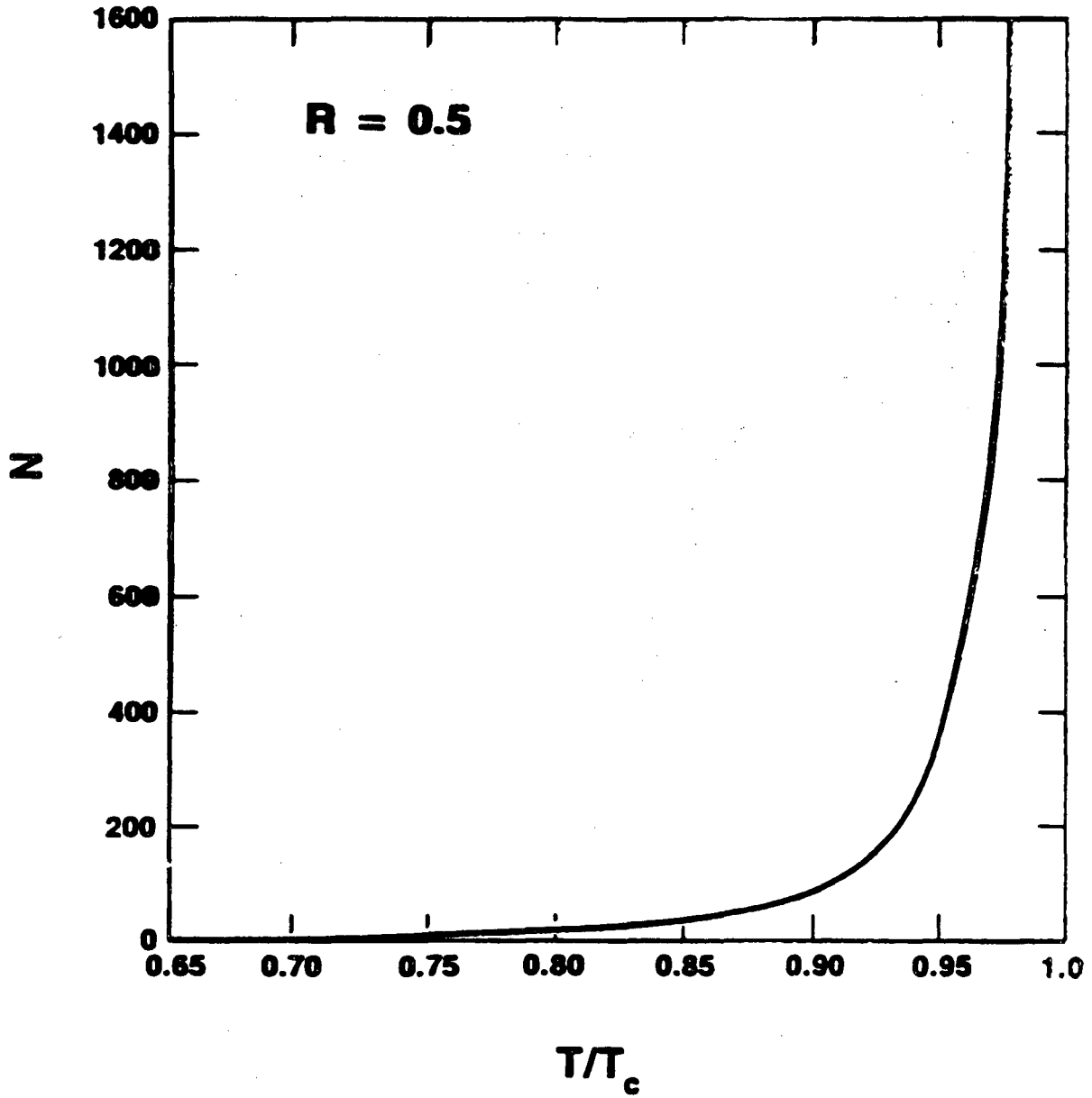


Fig. 4

XBL 838-2992

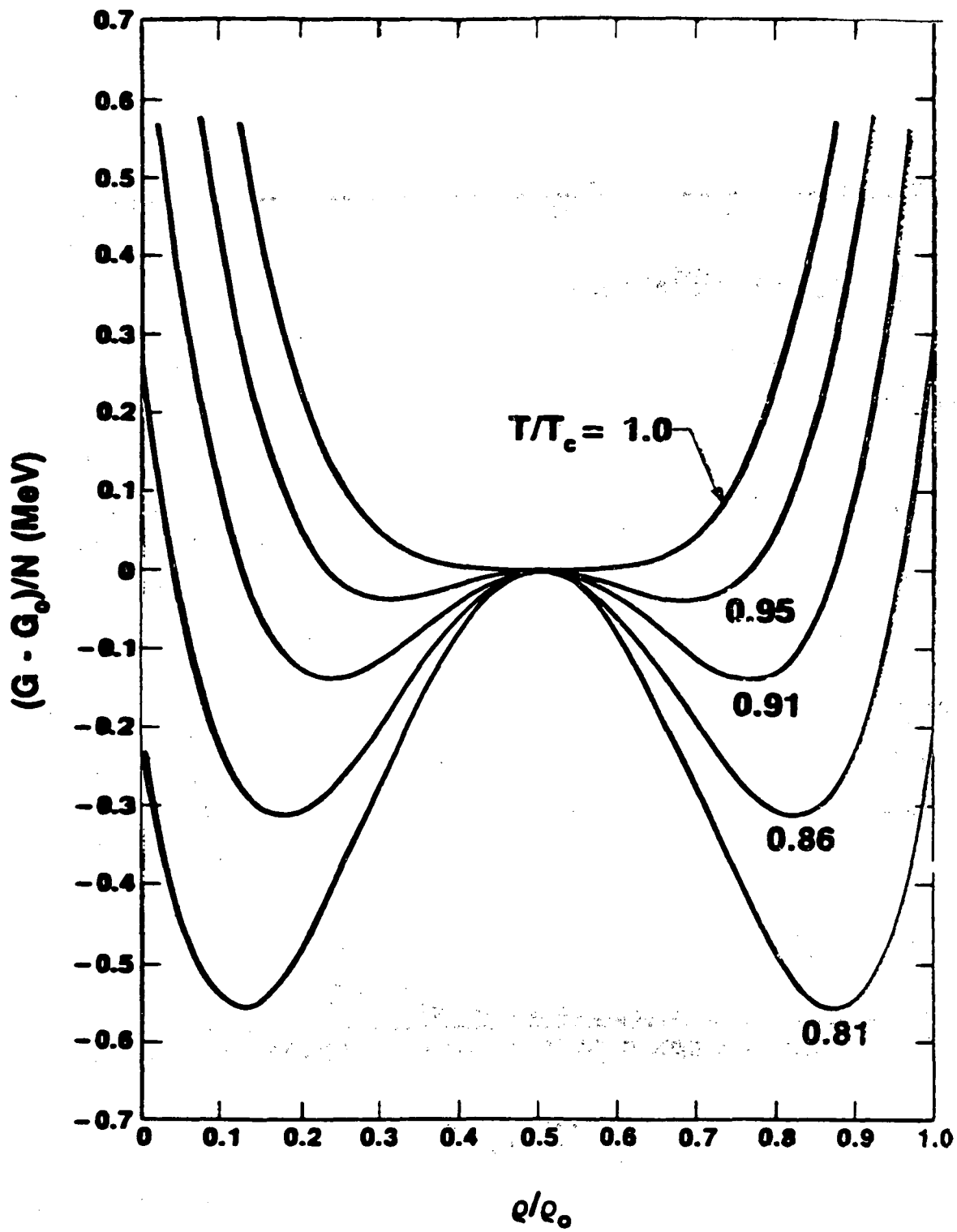


Fig. 5

XBL 838-2903

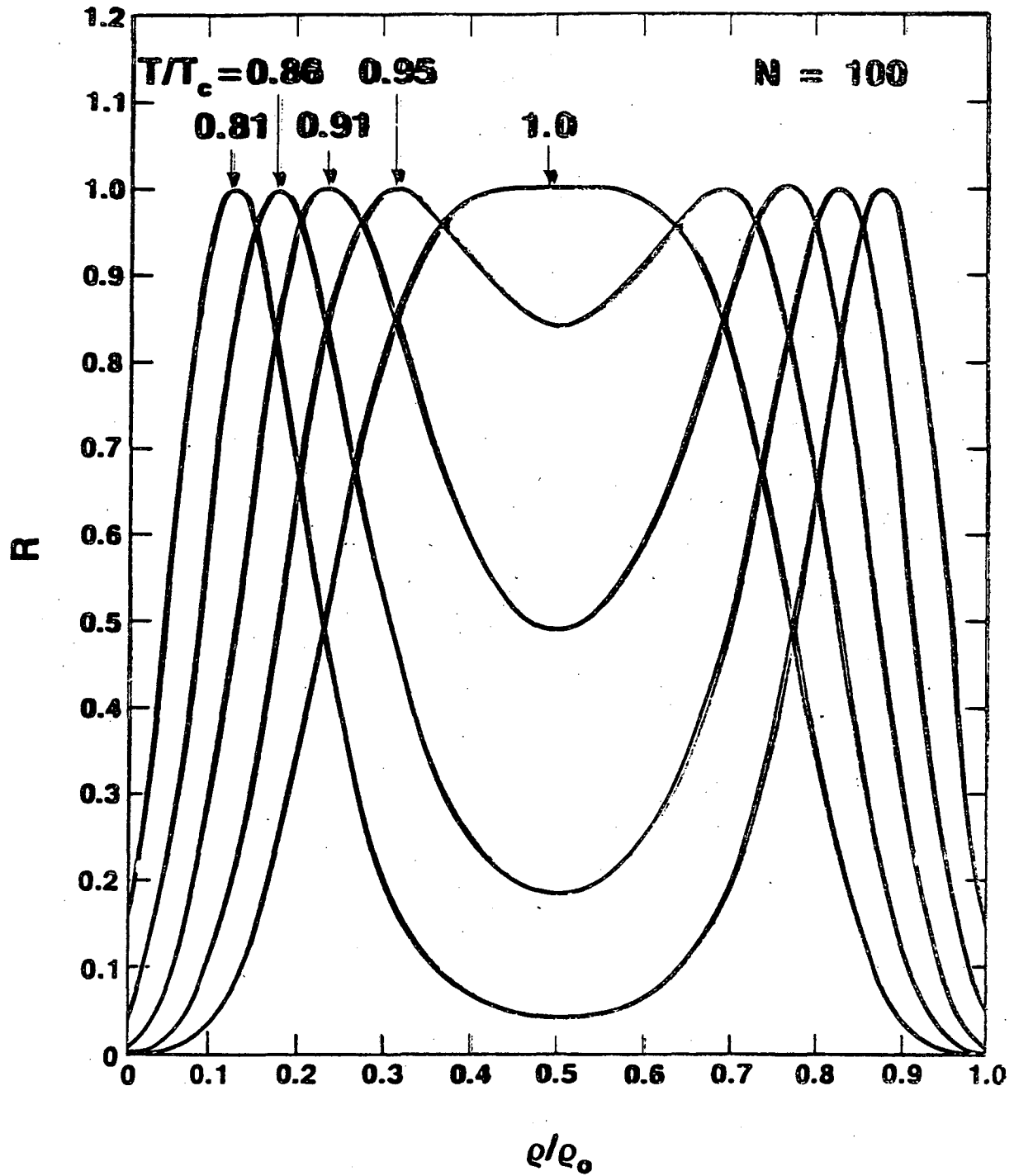


Fig. 6

XBL 838-2958

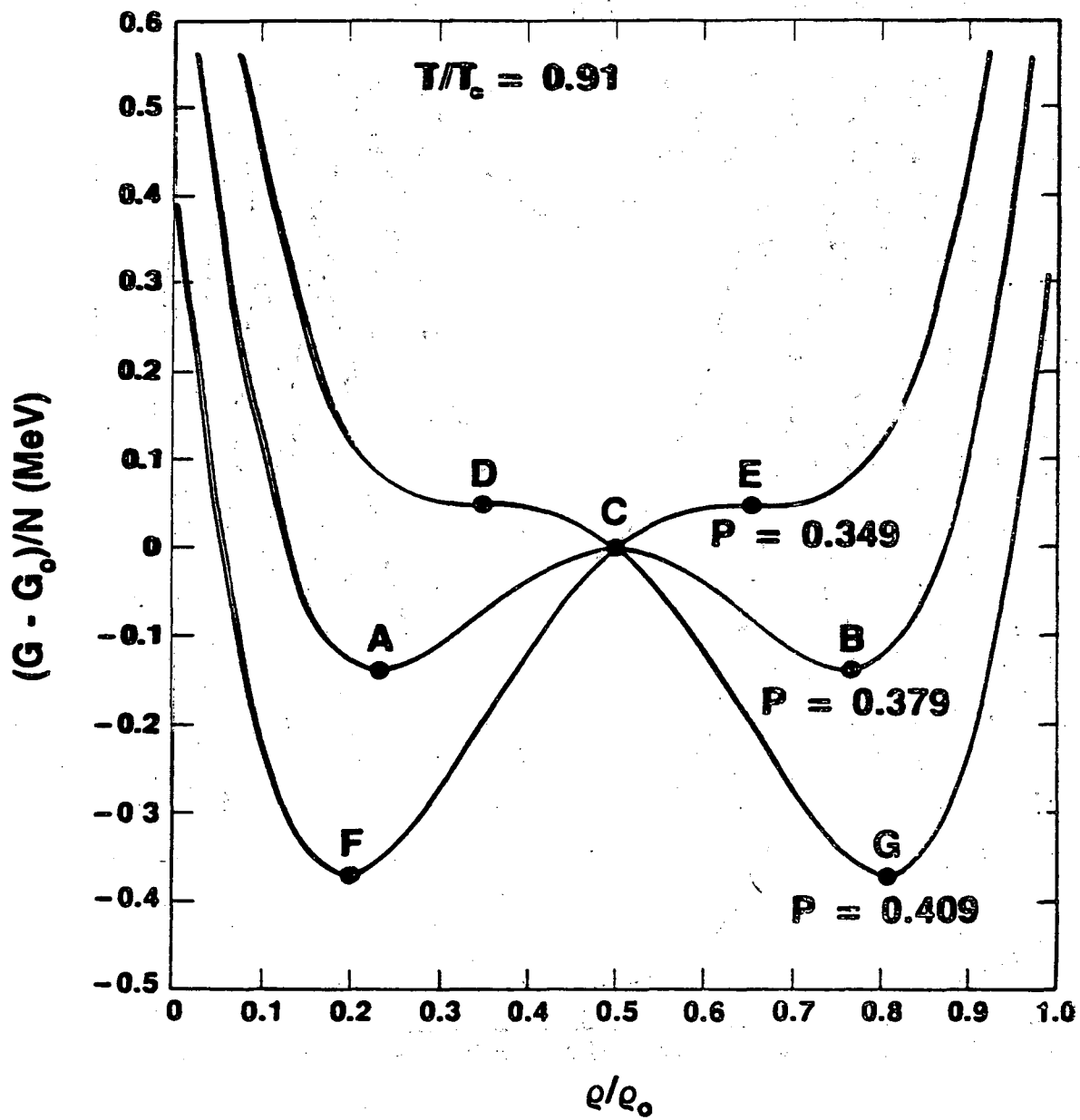


Fig. 7

XBL 838-2987

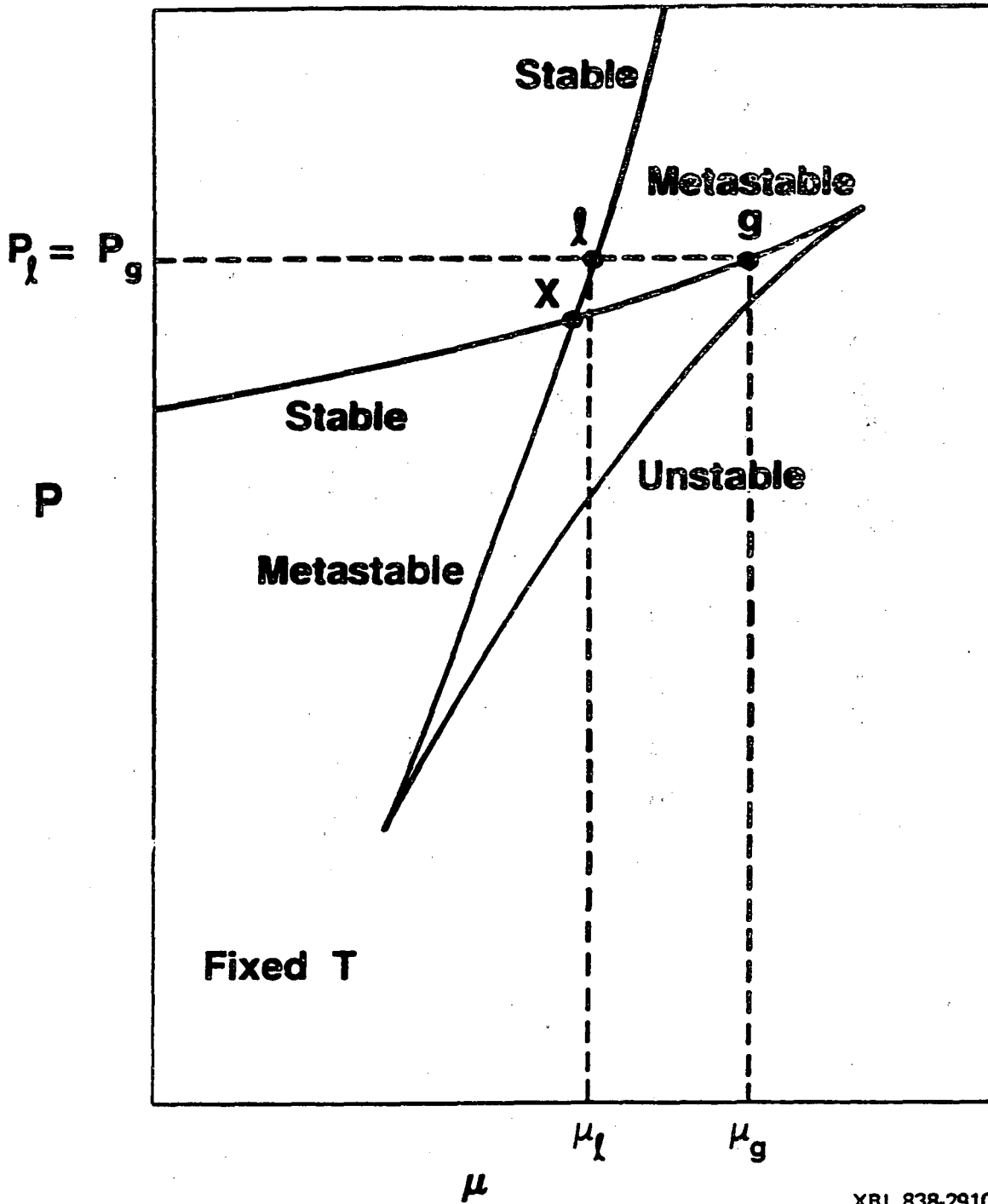


Fig. 8

XBL 838-2910

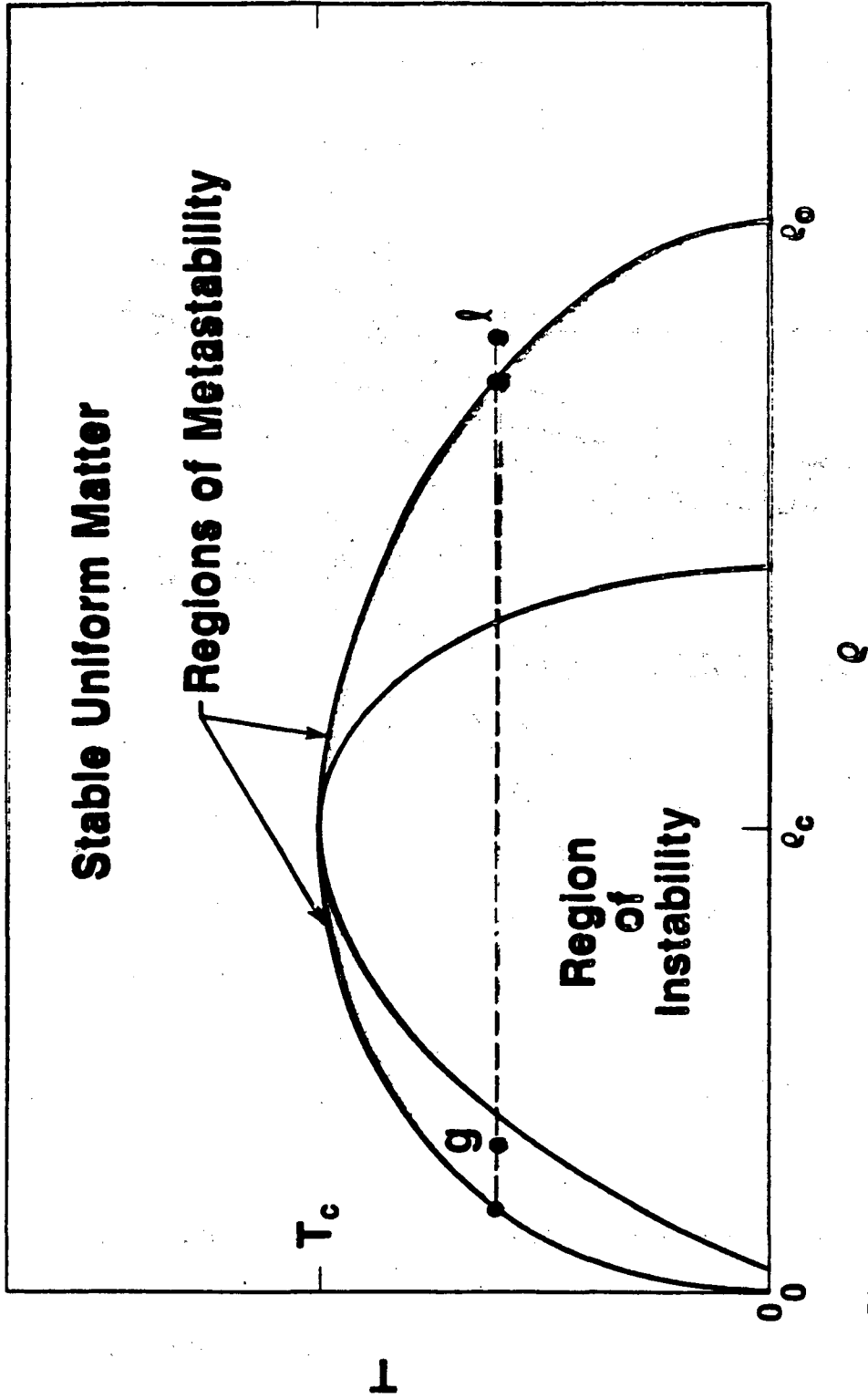


Fig. 9

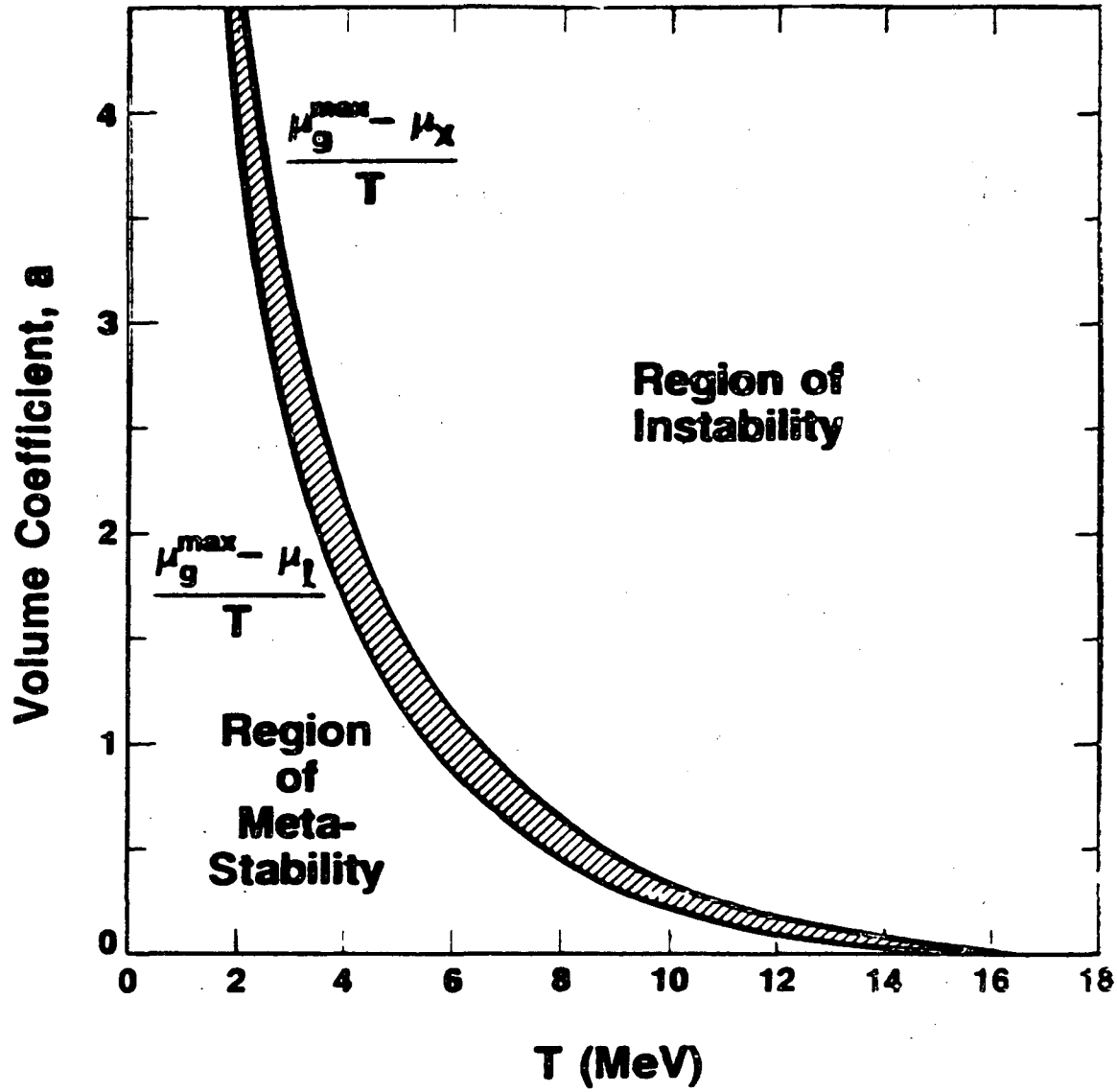


Fig. 10

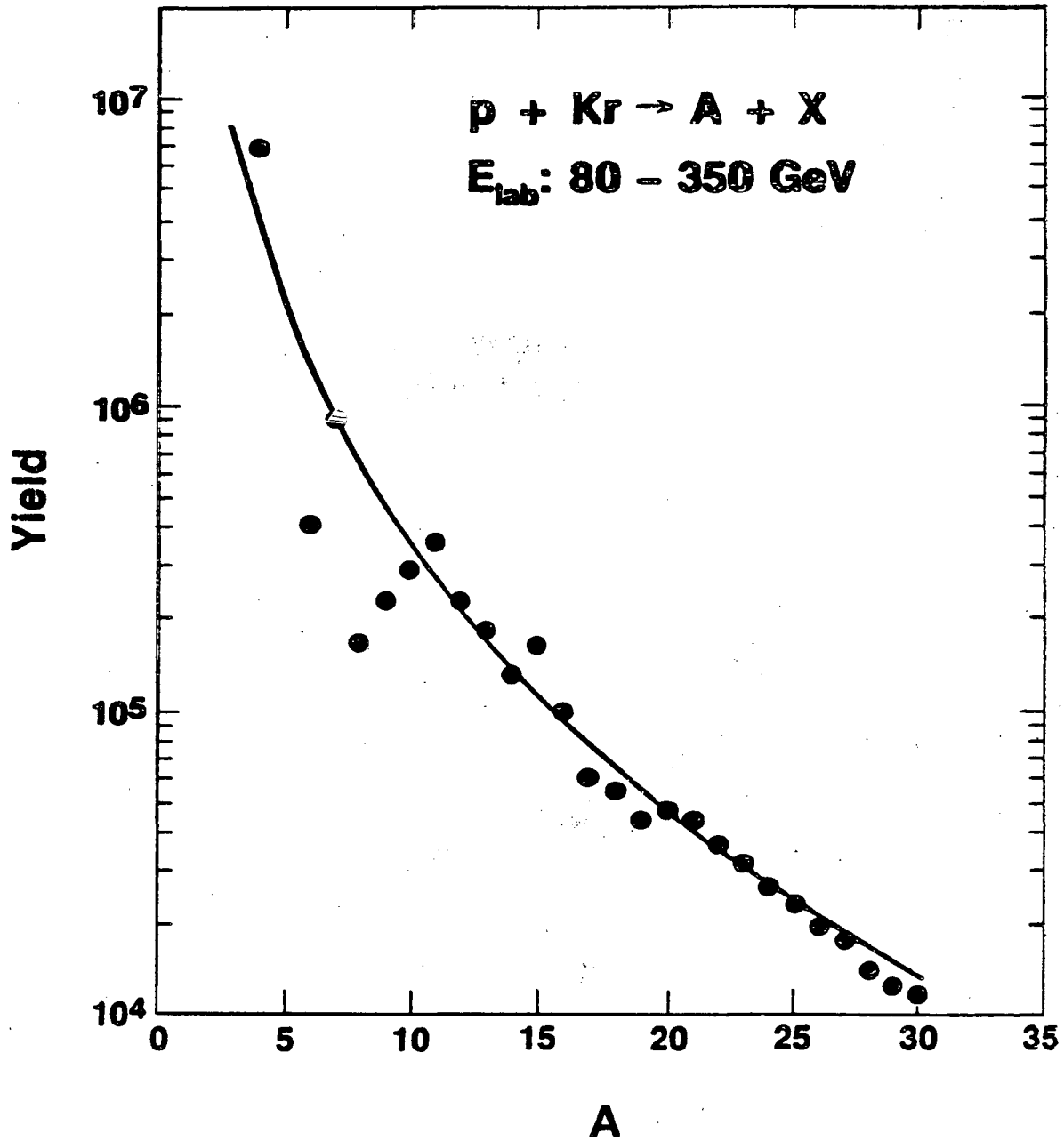


Fig. 11

XBL 838-2913

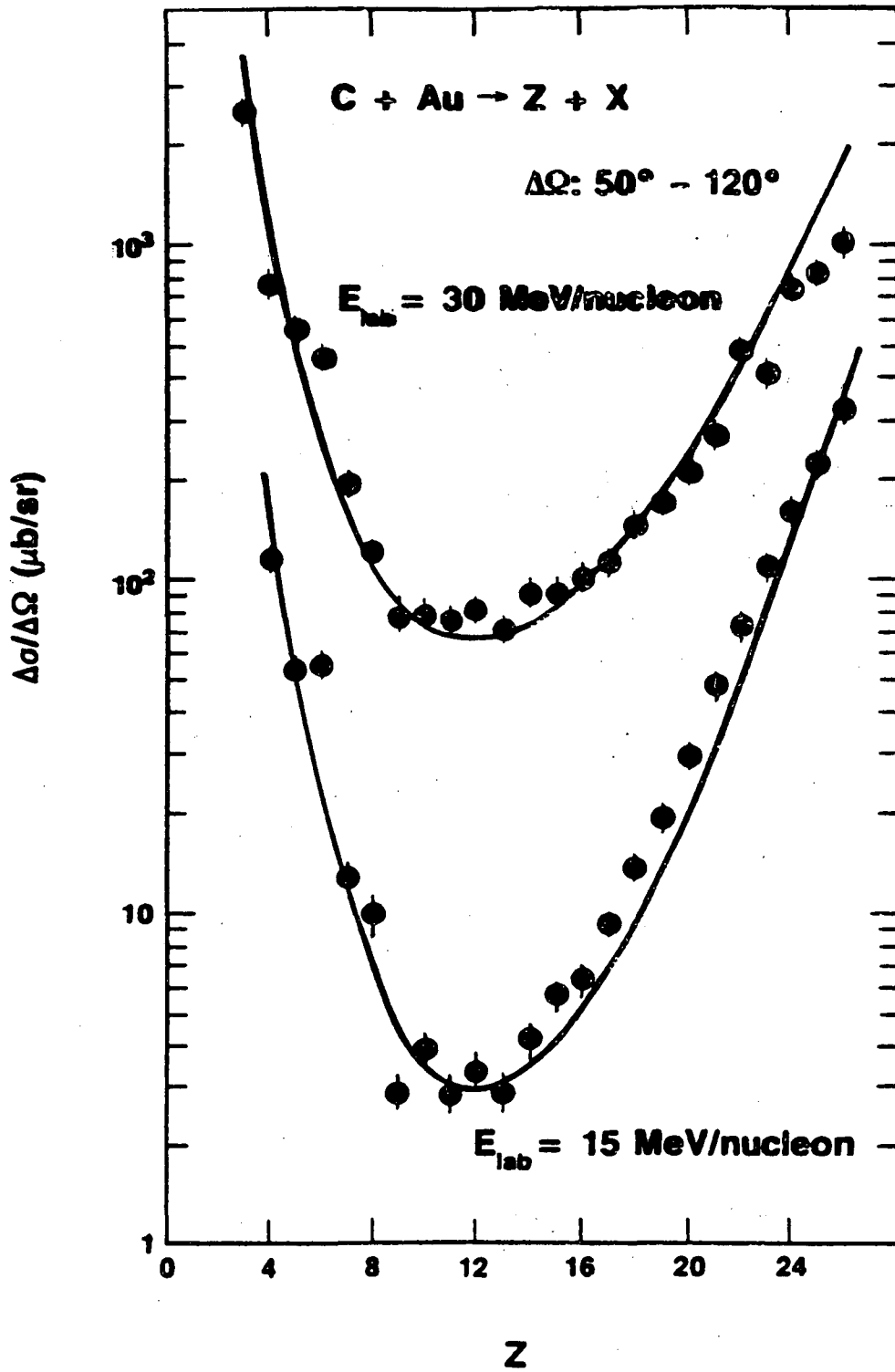


Fig. 12

XBL 838-2909

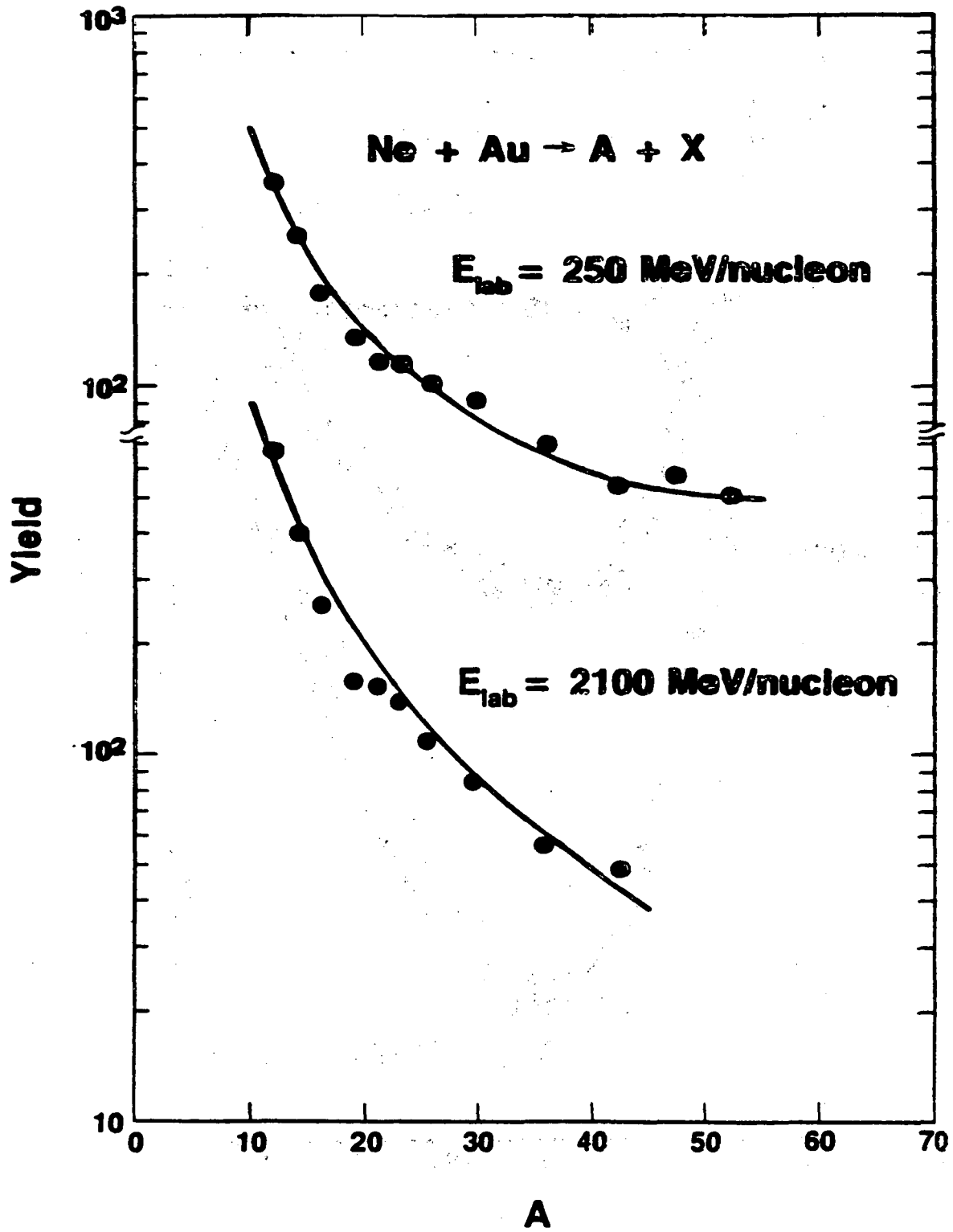


Fig. 13

XBL 838-2912

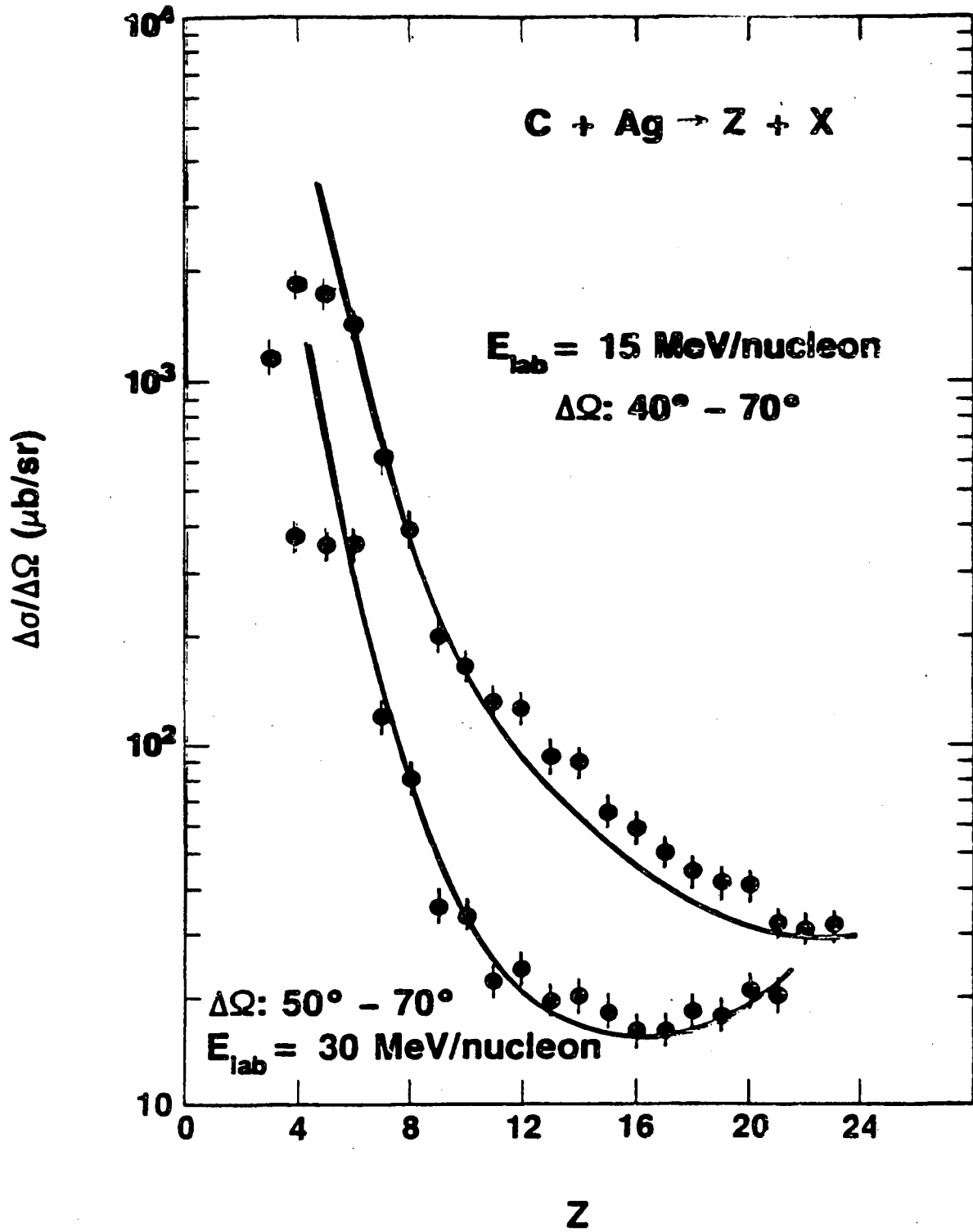


Fig. 14

XBL 838-2914

This report was done with support from the Department of Energy. Any conclusions or opinions expressed in this report represent solely those of the author(s) and not necessarily those of The Regents of the University of California, the Lawrence Berkeley Laboratory or the Department of Energy.

Reference to a company or product name does not imply approval or recommendation of the product by the University of California or the U.S. Department of Energy to the exclusion of others that may be suitable.

TECHNICAL INFORMATION DEPARTMENT
LAWRENCE BERKELEY LABORATORY
UNIVERSITY OF CALIFORNIA
BERKELEY, CALIFORNIA 94720